UNIVERSITY OF THE PELOPONNESE

FRAGKOU ATHANASIA

(R.N. 1012201502013)

DIPLOMA THESIS:

A micro-XRF investigation on the bronze statue of Poseidon of Livadostra

SUPERVISING COMMITTEE:

- Dr. Vasiliki Kantarelou

- Dr. Georgianna Moraitou

EXAMINATION COMMITTEE:

- Dr. Vasiliki Kantarelou

- Dr. Georgianna Moraitou

- Dr. Andreas - Germanos Karydas

KALAMATA, SEPTEMBER 2016

Contents

1. Abstract

This dissertation aims to present and interpret the results that were obtained by the micro-XRF analysis of the bronze statue of Poseidon of Livadostra before its temporary exhibition at the National Archaeological Museum at Athens. The bronze statue of Poseidon is an indicative example of the transitional period from the late archaic years to the early classical ones, and one of the few examples of this characteristic period that have been preserved and analyzed. The scope of the micro - XRF analysis was to answer specific analytical questions raised by the Head of the Laboratory of Conservation and the laboratory personnel related to its technical characteristics and state of preservation, namely the chemical composition of the different parts of the statue of Poseidon, to identify residues of past conservation treatments and better clarify the composition of the patina layer.

2. Acknowledgements

I would like to thank and express my gratitude to Dr. Georgianna Moraitou (National Archaeological Museum), Dr. Andreas-Germanos Karydas (NCSR Demokritos) and especially Dr. Vasiliki Kantarelou (NCSR Demokritos), for all their support and guidance during all the phases of the present dissertation. I would also like to thank the personnel of the Laboratory of Conservation of Bronzes of the National Archaeological Museum for their assistance during the in-situ analyses of the bronze statue of Poseidon. At the end, I would like to express my sincere gratitude to professor Nikolaos Zacharias for his overall guidance during the last year, and to the rest of the CultTech personnel, especially Ms. Vasiliki Valantou and Ms. Eleni Palamara for all their help and advice when needed.

3. Introduction

The purpose of this study is the presentation, evaluation and interpretation of the results that were obtained by the micro X-ray Fluorescence analysis of the ancient bronze statue of Poseidon of Livadostra. The analysis of the statue was undertaken upon request of the Head of the Laboratory of Conservation and Archaeometry of the National Archaeological Museum at Athens, Dr. Georgianna Moraitou, in collaboration with the Head of the X-Ray Fluorescence Laboratory of the National Center for Scientific Research, Andreas- Germanos Karydas, and Dr. Vasiliki Kantarelou. The aim of this study is to answer the certain analytical questions that were raised by Dr. Georgianna Moraitou and the laboratory personnel, related to its technical characteristics and state of preservation. The principle of operation of the X-Ray Fluorescence technique and its contribution in the study of metal alloys together with information on ancient copper metallurgy and with the archaeological and historical background of the statue will be reviewed in the chapters 4-6. The analytical methodology that was followed during the measurement campaign and data analysis is comprehensively presented in chapter 7. The last chapter is dedicated to the interpretation and discussion of the results, together with the general conclusions that were drawn from the study of the bronze statue of Poseidon of Livadostra.
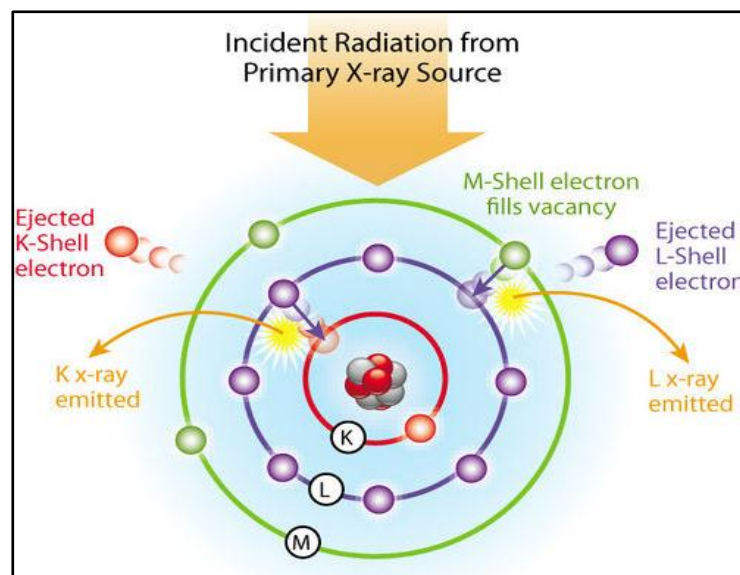
4. X-Ray Fluorescence

The X-Ray Fluorescence technique is a firmly established and widely used analytical tool in the field of archaeological science for the past few decades due to its attributable characteristics. It is a non-destructive method that requires no sample preparation and where the analysis is conducted no alteration in the integrity of the surface microstructure is observed. It is characterized by its high analytical sensitivity (mostly in medium Z elements), and in principle when it is applied in the field it can detect the vast majority of elements on the periodic table, namely from the atomic number Z=11 to Z= 92.

In the field of Cultural Heritage, the X-Ray Fluorescence technique is applicable to different kind of materials such as ceramics, glasses, metallic alloys, pigments etc. It provides generally rapid analyses, with a few seconds being enough time for the analysis of metallic alloys. The portability of XRF spectrometers consists a very advantageous feature which greatly facilitates the scientific examination of museum objects, since they cannot always be transported to the laboratory because of their size or value, or because the transportation may cause strain to the object and have an adverse effect on its preservation state. (Janssens, et al., 2000) (Karydas, 2007).

4.1 Basic principal of the XRF technique

The X-Ray Fluorescence method is based on the ionization of the atoms of the material when it is irradiated by an energetic beam of primary X-rays. X-rays is electromagnetic radiation of very short wavelength that ranges between 0.1 and 10 nm, and of adequately high energy to be energetically able to expel inner-shell electrons from the atomic shell. X-rays can be produced by using an X-ray tube, radioisotopes or synchrotrons. After the energy of the beam is absorbed by the atom, an inner-shell vacancy is created and that brings the atom to an excited state. As it returns to its primary energy condition, an electron from an outer-shell occupies the vacancy that was created by the ionization and while this happens, a characteristic secondary X-ray can be emitted. The energy of the photon is equal to the energy difference of the two shells involved in the transition. Since every element has a unique set of energy levels, its X-ray emission spectrum will be also characteristic, whereas the intensity of the emission X-ray lines is related to its abundance within the analyzed sample. An energy dispersive X-ray detection system has the potential to record the energies of the emitted characteristic X-rays and by this way a qualitative elemental analysis of the measured sample can be achieved (Karydas, 2007) (Van Grieken & Markowicz, 2002).

Figure 1. *The interaction of the primary set X-rays with the atom and the production of the secondary set of X-rays (source:* https://www.911metallurgist.com/blog*)*

4.2 The role of XRF in the analysis of ancient alloys

The X-ray Fluorescence technique is a highly-appreciated tool for the study of metallic surfaces (Janssens, et al., 2000) since it can offer a great insight on the elemental composition of an alloy when there are no corrosion products on the surface of the object.

The compositional profile of ancient copper alloys through different chronological periods can reveal specific chemical patterns that could support a first attempt to suggest or confirm a specific period of their manufacture (Karydas, 2007). The various differences between metal alloys, for instance the presence of an element, and the ratio between the alloying elements, may vary from era to era and from one region to another, depending on the availability of raw material resources, on the price of the metal, which in most cases was in proportion to its availability and demand, and on the purpose that the object would serve, functional or decorative (Liritzis & Zacharias, 2011). Moreover, when quantitative results are examined, the random presence of a metal in the ore can be differentiated from its deliberate use, when its concentration does not exceed approximately more than 2-3%[1].

The XRF technique can also help to resolve authenticity issues related to ancient alloys through the determination of the abundance of its constituent elements. Since some metals were used in certain time periods or certain geographical contexts, and their concentration of that time is already known, then the classification of the object can be done (Ferretti, 2014). A great example is the study of ancient Greek bronze statues and their Roman copies. In Roman times, the mean value of the lead content in bronze statuary exceeds the one of the ancient Greek, and that is an indicator that a statue can be a roman copy of a Greek original (Caley, 1951).

The XRF analysis can be also used to assist in the identification of the presence of certain corrosion products. It is important though to mention that since XRF is an elemental analysis technique and cannot detect chemical compounds, the various corrosion products cannot be specifically identified, but simply suggested with the support of elemental associations observed at the microscale, the macroscopic/

---

[1] This is a matter of debate in some cases, since there are ores that were used in antiquity for the production of statuary, and they were rich in elements such as zinc, but the craftsmen were not aware of that fact, thus the presence of this element cannot be considered intentional (Craddock, 2009).

microscopic documentation of their surface, the color hue of the analyzed surface, etc. The characterization of corrosion products helps to better understand the conditions of burial or the degree of damage that parts of the object have undergone.

Some advanced methodologies have been proposed by means of XRF analysis to identify those surfaces of bronze alloys that have undergone a kind of alteration and the formation of a corrosion layer. This can be achieved through the determination of the ratio between of the relative intensities between the SnKα and the SnLα X-ray lines from the measured areas (Gianoncelli & Kourousias, 2007) (Kantarelou, et al., 2007), in comparison with the ratio obtained from bronze reference materials (Kantarelou, et al., 2015). It is noted that the characteristic Sn-Lα X-rays having a much lower energy than the Sn-Kα characteristic X-rays originate from a more superficial layer and thus are more sensitive in the presence of a corrosion stratified layer. In order to get reliable and accurate quantitative data, the measured elements should be homogeneously distributed across the analyzed volume of the sample and this volume must be representative of the bulk composition of the object (Kantarelou, et al., 2007). Finally, during the interpretation of the spectra that have been acquired, attention must be given to overlapping peaks that can cause overestimation of one element and underestimation of another, as for instance in the case of the AsKα and PbLα X-ray emission lines that will be reviewed later on in this dissertation.

The XRF analysis can also reveal information related to the manufacture technology or previous conservation interventions. For example, for the cold working of bronze statues, a metal that would prevent gases from infiltrating the molten alloy such as tin and lead would be favorable. Moreover, welding and filling products which have been used in previous conservation treatments can be also analyzed and determined, but results will be obtained only if their components are inorganic.

The XRF technique is a valuable tool that can contribute a great deal in the compositional and generally characterization studies of metal alloys in combination with other available spectroscopic techniques such as XRD and FTIR which have been proven more suitable for the study of corrosion products. Conclusions however, must be always drawn by considering all other information concerning the

environmental conditions that the object has been exposed to, such as the burial or the museum environment.

5. Ancient copper metallurgy

5.1 Copper alloys used in ancient Greek statuary

One of the most widely used alloys in antiquity was bronze. Bronze was used for producing a wide range of objects from everyday household items that had functional purpose to the manufacturing of armors and weaponry. Bronze was also a highly-appreciated alloy for the production of statuary and though not many ancient Greek bronze statues have survived until our times, the ones remaining provide us with a great deal of information about the manufacturing techniques and the quality of the bronze work of that time (Mattusch, 1988).

Bronze is an alloy consisting primarily of copper and tin. Throughout the Greek antiquity, the percentage of tin and copper in bronze statuary remained fairly constant, with the tin content not exceeding 15% (Craddock , 1977). Tin was added to copper so as to decrease its melting point. It is characteristic that copper melts at 1083 ℃, but with the addition of 7% tin this melting point can be decreased to 1050 ℃, and even to 1020 ℃ with the addition of 10% tin. This means that bronze requires less heat in order to be kept liquid while working with it. Molten copper has also the ability to absorb gases and thus it cannot flow that freely in the mould, so the cast metal can be potentially disfigured with blow-holes. The addition of tin can significantly reduce this danger and also it can improve the mechanical properties of the metal. A bronze alloy with a concentration of more than 5% tin, has a reddish tint because of the copper content, but as time passes, it gains a golden-brown hue. The concentration of tin though is advisable not to overcome 15% in statuary otherwise its brittleness will also increase (Haynes, 1992).

Another metal that can be added to a copper - tin alloy is lead. Lead has also the ability to bring down the melting point of the alloy, and it improves its fluidity and resistance to the infiltration of gases while working on the cold state. Lead though, has also the drawback that during solidification, it separates from the rest of the mixture and it forms individual granules that may threat the structural cohesion of the statue. Lead in ancient Greek bronze work could be added intentionally in the alloy or it could be found in traces as an impurity because of its presence in the ore. The intentional use of lead throughout antiquity was up to 9%, with some rare

examples reaching up to a 20% concentration of lead as the production of statuary proceeded in time (Craddock , 1977).

Zinc can also be found in copper – tin alloys and as the above-mentioned elements, it also has the ability to lower the melting point of the alloy. Moreover, zinc offered protection against the absorption of gases. Alloys that contain copper and more than 30% of zinc are called brasses (Haynes, 1992).

In ancient Greek bronzework, another element that can be also found is iron. Iron can be found in small traces in copper ores or can be added intentionally, also in small amounts as part of the smelting process. In ancient Greek statuary iron, does not exceed 1.6%, with the already existing data, because its presence in larger amounts would make the metal hard to work with (Craddock & Meeks, 1987).

Manganese is another metal that was added in small quantities in antiquity so as to increase the viscosity of the molten alloy. Apart from being deliberately added, it can also be found as an impurity of the ore.

Other elements that can be found in bronzes are nickel, bismuth, arsenic and silver, but usually in concentrations that do not exceed 1%, thus they can be considered as impurities at the ore (Haynes, 1992). In the study of ancient bronzes, it is useful to estimate whether a component of the alloy was added intentionally, or was randomly used because of its presence in the ore, because that can lead to conclusions about the use and distribution of ancient metals and the manufacturing techniques.

6. Poseidon of Livadostra

6.1 Historical & archaeological context

The bronze statue of Poseidon was discovered in 1897 laying near the shore, in waters less than a meter deep in the cove of Ayios Vasilios in Boeotia, Greece. In ancient times Ayios Vasilios served as the port of Platea, since the bay opens to the Corinthian Gulf (Aravatinos, et al., 2003), and many scholars associate the discovery of the statue in this area with the existence of an ancient temple dedicated to Poseidon. The statue was found by local peasants heavily corroded and mutilated, laying in nineteen pieces at the bottom of the shallow waters of the bay, and it was identified as Poseidon by an inscription found at the bottom left of the bronze base that the statue was fixed upon, that reads "Sacred to Poseidon" (*Το Ποτειδάονος ἱαρός*). So far no physical indications have been found that can explain why or how the statue ended up in the sea, but it can be attributed both to natural and human forces.
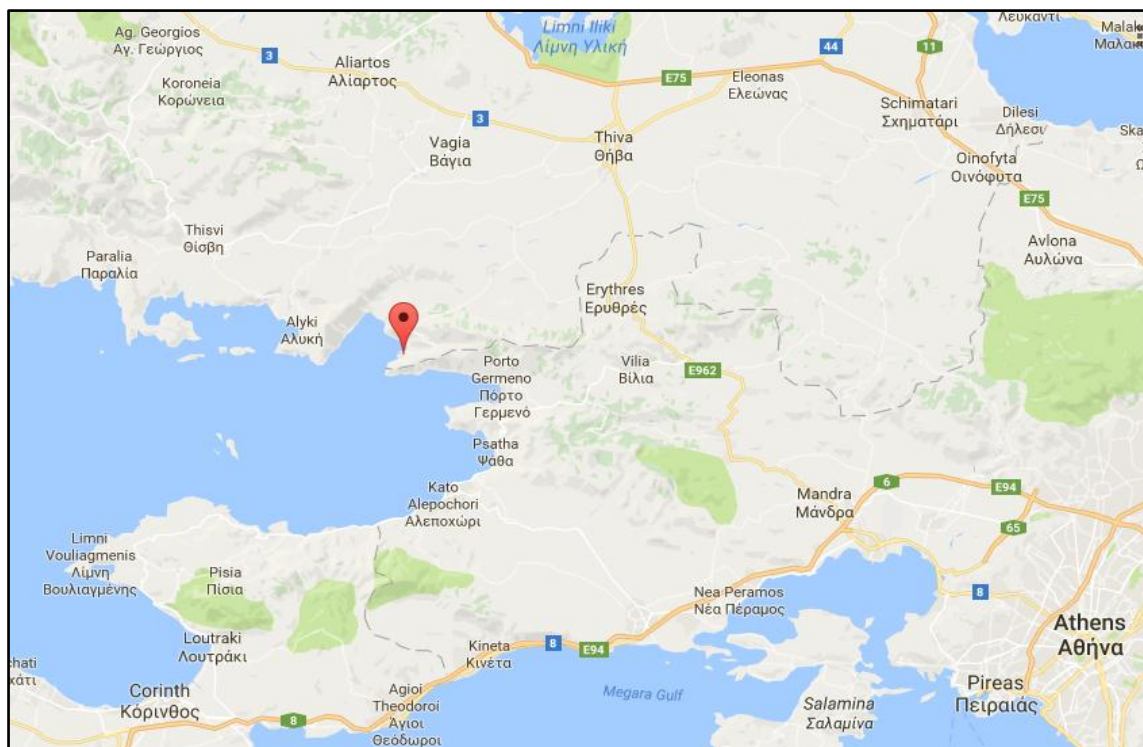
Figure 2. Map of the area where Poseidon was discovered © Google Maps.

The most prevailing speculations are that the statue was either thrown to the sea by human forces thus, by the early Christians in the transitional period from the ancient Greek religion to Christianity or by natural forces. There is one natural force that can be associated with Poseidon being thrown at the sea, and that is a severe earthquake that occurred in the area in 373 BC which was responsible for the destruction of the ancient city of Helike and for the destruction of the temple of Apollo at Delphi that is situated not far to the northwest of the bay where the statue of Poseidon was recovered (Houser, 1983). The archaeologist who studied the statue back in the late 19th century suggests that it could have also been thrown to the sea by the soldiers of Mardonius after their retreat in the battle of Platea in 479 BC (Philios, 1899).

Figure 3. The bronze statue of Poseidon after the conservation treatment for its temporary exhibition at the National Archaeological Museum at Athens. © Archaeological Receipts Fund/ Photo taken by Galanopoulos, 2016.

The statue dates back approximately to 480 BC and is an indicative example of the transitional period from the late archaic years to the early classical ones (Kaltsas, 2007). 480 BC was an important year that marked the end of the Persian wars, and played an important role in the production of statuary and in the distribution of raw materials.   The bronze statue has a frontal position that resembles the one of a Kouros, since it directly confronts the viewer, but in this case the right foot is in advance. The body is characterized by its naturalism and it has a slight torsion to the left, since the weight is planted on the left foot. Part of the central and left side of the chest is missing, but the gaps that once hosted the inlaid nipples probably from copper are still visible. Part of the right leg is missing from below the knee until sole of the foot. Though both arms have been also long gone, the remaining pieces indicate that once the right arm was extended forward and the left one was probably raised and drawn back to carry a weapon, probably a trident.
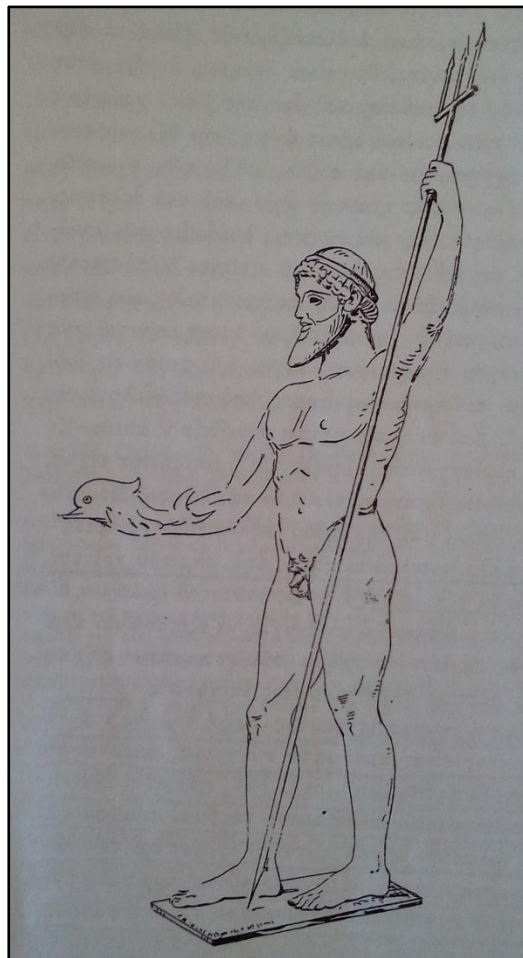
Figure 4. *Sketch of how the original appearance of the statue may have looked like by E. Gillieron (late 19th century).*

The head that was found detached from the rest of the body but in a much better condition, is also more stylized part of the statue. It consists of a beard that begins from beneath the ears, following the line of the cheekbones, while it surrounds the lips and reaches until the upper chest of the statue, in a course that resembles a spade, and it is carved with groups of delicate wavy lines, interspersed harmoniously by a deeper wavy channel. The hair begins from the crown of the head and is incised, but more vividly in comparison to the beard, with groups of fine wavy lines divided by regularly spaced deeper lines (Mattusch, 1988). The eyes, eyebrows and lips were all inlaid, and today only the left eyebrow and the lips have survived.

Figure 5. Close photo of the face of the statue after the conservation treatment for its temporary exhibition at the National Archaeological Museum at Athens. © Archaeological Receipts Fund/ Photo taken by Galanopoulos, 2016.

During the assemblage of the statue back in 1899, it was discovered that the head had been detached from the rest of the body at least once before, during the ancient years, because the area in which the head would be joined with the rest of the body had been smoothed out, probably with mechanical means, due to geometry issues that may had arisen back at that times.

The attribution of the creation of the statue to a specific workshop is not determined with the existing data, and opinions seem to vary even to a possible location of manufacturing. Philios, the archaeologist who published the findings concerning the statue back in 1899, suggests that an Athenian workshop might have been responsible for its creation, since Athenians had the expertise and the personnel back at that time to create a work like Poseidon. In his study though, he does not rule out other workshops from Aegina, Boeotia and Sikyon. Philios also suggested that Poseidon is a product of the Archaic era and dated it back approximately to 500 BC, a fact that he attributes to the inscription at the base of the statue. The evidence that led him to this assumption is the linguistic study on the inscription, that characterized the way the word Poseidon is addressed as a Boeotian type characteristic of the Archaic years (Philios, 1899). This assumption though can be misleading, since the specific type could have been used for many years after the end of the archaic period and the transition from archaic to classical years does not mean necessarily that this term could have been abolished.

When it comes to the manufacturing technique, most scholars are in agreement and suggest that it was made by the indirect lost-wax process of manufacturing ancient Greek statues. The uniform thickness of the walls of the statue and the fact that the interior is smooth and regular without disruptions can be attributed to this particular technique (Mattusch, 1980) (Haynes, 1992).

6.2 Manufacturing Process

The indirect lost wax process was used particularly in the fifth century BC for the production of small and medium sized metal sculptures. At first, the craftsman carved a figure, one that would resemble the final sculpture, in solid wax and then he would cut it separately into pieces such as torso, head, arms and legs (Fig. 6_A). In order to make a hollow duplicate of the original the craftsman created a mould (Fig. 6_B) and then took impression of each part of every section by embedding the piece in clay and then poured liquid plaster into the exposed area of the mould in order to form one part. Afterwards, he would assemble these two pieces together and he would fill the section with hot wax (Fig. 6_C). When the hot wax came in contact with the cold plaster it hardened into a thin shell and the excess liquid wax was poured out (Fig. 6_D). When the wax cooled, the craftsman opened the mould and a hollow wax duplicate of the original section was created (Fig. 6_E). The core of the section was then filled with a mixture of sand and clay and iron pins were inserted through the wax shell in order to hold the mixture of clay in place (Fig. 6_F). The next step was to create a circulatory system for the molten bronze to flow and this was accomplished by creating a network of solid wax roads attached to various parts of the figure (Fig. 6_G). This network also acted as a vent for gasses to escape after the bronze was poured to the mould. This ensemble was then encased in an outer mould with an opening at the top (Fig. 6_H) and then it was turned upside down and was heated for the wax to melt and leave the mould (Fig. 6_I). The mould was ready for casting and the molten bronze was then poured through the opening and filled the empty channels that had been created when the wax was poured out (Fig. 6_J). When the bronze alloy was cooled down and became solid the mould was broken open. This procedure happened for every section of the body and after the various parts of the statue were created, the bronze worker would do some cold work, for instance remove the channels and the core pins that were holding the clay model and also by removing any unnecessary products from the surface of the statue (Fig. 6_K). All the sections then would be joined together by mechanical or metallurgical means. In areas that had undergone damages or displacements during the breaking of the final mould, the worker would add on top a patch so as to cover it for aesthetic purposes (Fig. 6_L). At the end, before the statue being polished, it could be mounted at a base if needed, that

was accomplished by creating vacancies in the soles of the feet and the base and then joining them together by filling these vacancies with lead (Haynes, 1992).
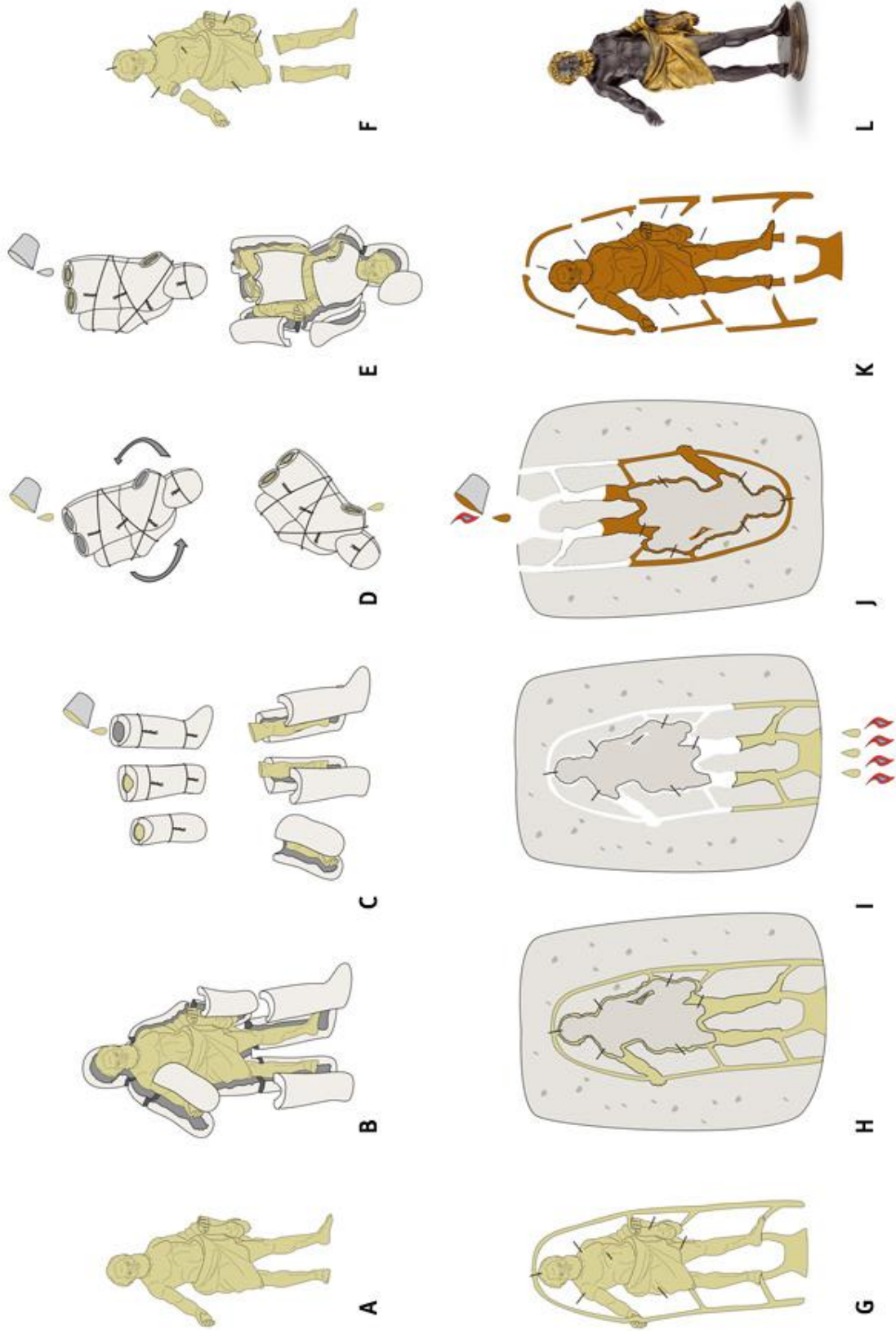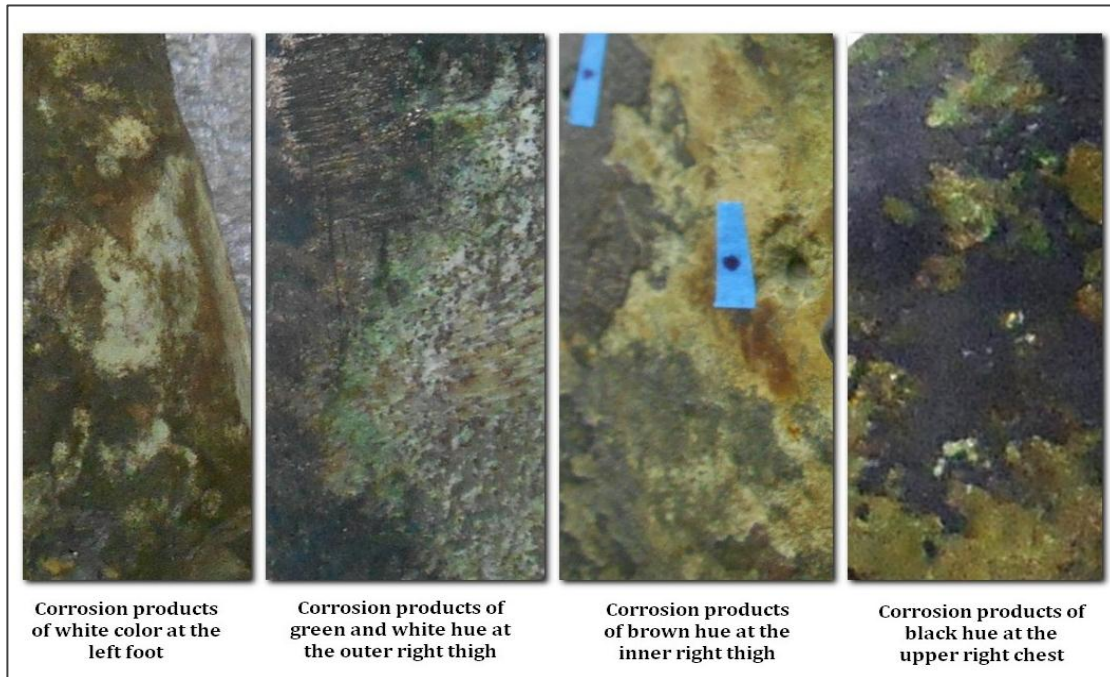
Figure 6. The indirect lost wax process in steps. Photo taken by Antico: The Golden Age of Renaissance Bronzes and it represents a bronze statue of Hercules that was casted around 1496. The Frick Collection, New York.

6.3 State of Preservation[2]

By just macroscopically observing the statue several conclusions can be drawn. Firstly, the surface is rough with many dents and heavily corroded with areas of white, green, brown and black hue (fig 7). These areas can be clustered accordingly to their color and this differentiation can be attributed to the various corrosion products. Most of the corrosion products that can be found nowadays at the surface of the statue are attributed to the museum environment and a small amount to the marine environment, because most of them have been removed during the previous conservation treatments. A characteristic example is that during the days of the analysis of the statue the inscription that is located at the support base could not be distinguished. Another corrosion product that can be found in several areas of the body, such as the head and legs, are copper platings with irregular shape and size (fig 8). Copper platings are created in bronzes from the reduction process of copper which leads to the creation of areas with high concentration of copper. Throughout the surface of the statue several nails, patches and copper platings can be also found. A small amount of the nails and patches present can be attributed to the manufacturing process, and were used in order to join the various parts of the statue, but most of them were used in the first conservation treatment in the end of the 19th century in order to put the various parts of the statue back together. It is also important to mention that the statue had been conserved three times before the analysis. The first time was after it was unearthed from the bottom of the sea at the end of the 19th century and then two more times around the 1930s (fig. 9) and 1970s. No record has been found so far that can give us a clue about these previous conservation treatments.

---

[2] The present subsection refers to the preservation condition of the statue during the time of the analysis and is included in order to give the reader a better understanding of the conditions during the time of the analysis. After the analysis was carried out, the statue was conserved by the museum personnel for its temporary exhibition.

| Corrosion products of white color at the left foot | Corrosion products of green and white hue at the outer right thigh | Corrosion products of brown hue at the inner right thigh | Corrosion products of black hue at the upper right chest |

Figure 7. Example of various corrosion products found on the surface of the statue

| Copper plating, back of the head | Copper plating, right leg | Copper plating, back of the head | Copper plating, left leg |

Figure 8. Example of copper platings throughout the surface of the statue
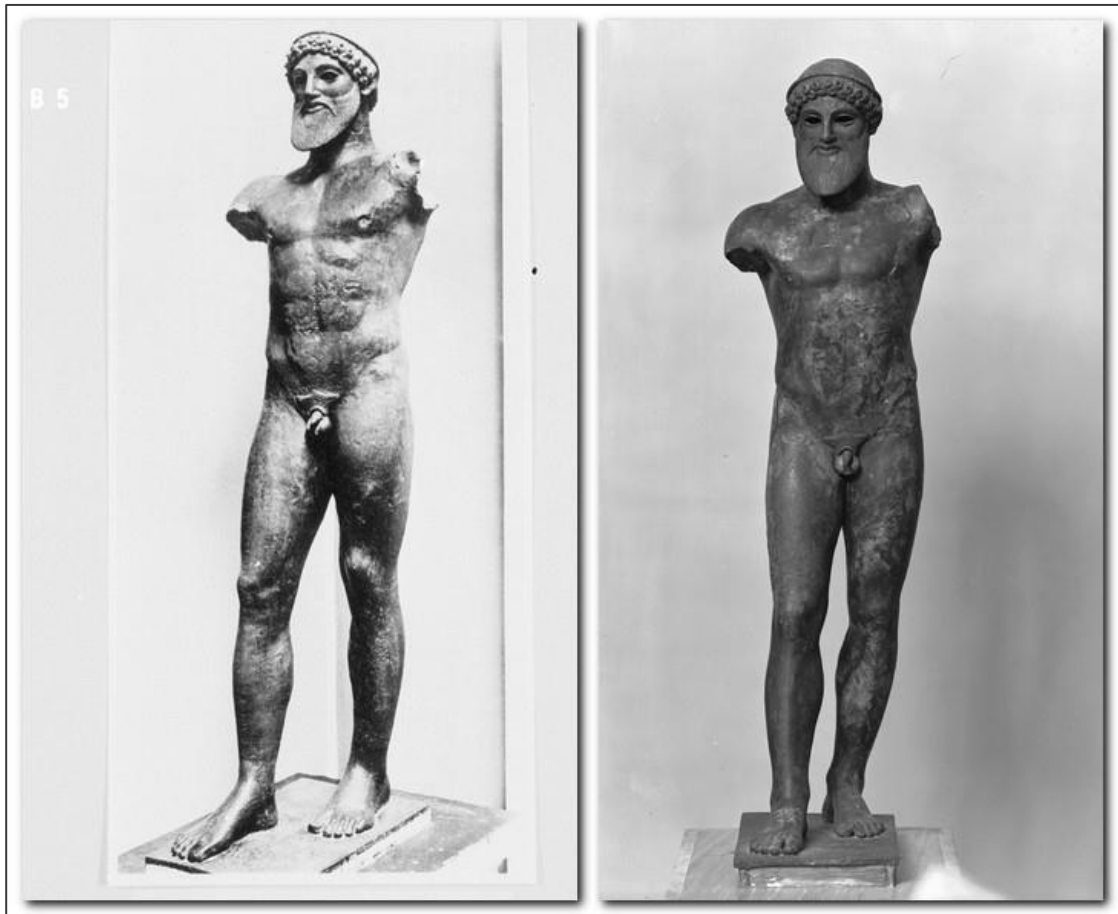
Figure 9. The statue of Poseidon around the 1930s © Rechte vorbehalten - Freier Zugang (source: http://www.bildindex.de/document/obj20322605?medium=fm134189, accessed October 2016)

7. Experimental

7.1 Materials and methods

7.1.1 Micro-XRF spectrometer

The examination of the Poseidon of Livadostra was conducted in the Laboratory of Conservation of Bronze Artefacts of the National Archaeological Museum of Athens, by using the portable micro - XRF instrument of the Institute of Nuclear and Particle Physics of the NCSR Demokritos. The INP μXRF is a customized version of the commercial μXRF spectrometer Artax (Bruker-Nano). The spectrometer probe consists of an X-ray micro focus Rh-anode tube (spot size 50μm × 50μm, 50 kV, 0,6 mA, 30 W maximum power consumption with 0,2 mm Be window thickness) and a polycapillary X-ray lens as a focusing optical element that offers a focal distance of about 21mm and a spatial resolution in the range 40μm - 80μm, when the unfiltered tube radiation is used as an exciting X-ray beam. The X-ray detection chain consists of a thermo-electrically cooled 10mm^2 silicon drift detector (X-Flash, 1000B) with FWHM equal to 146 eV (at MnKα and 10kcps) coupled with a digital signal processor. The colored CCD camera that is attached to the spectrometer head can offer live documentary image of the analyzed spot, whereas together with a dimmable white LED for sample illumination and a laser beam indicator the reproducible positioning of the measuring probe with respect to the analyzed surface is guided. The head of the spectrometer is equipped with three stepping motors which facilitate its movement in three orthogonal directions, thus the analysis spot can be set precisely at the focal distance of the polycapillary lens and the possibility of an elemental mapping is also provided. All the above-mentioned parts are supported on a flexible head which can be also tilted at different orientations in order to better access curved areas and these overcoming limitations imposed by the geometry of the artefacts surface. (Kantarelou, et al., 2007) (Kantarelou, et al., 2015).

The flexible head of the μXRF spectrometer allowed the examination of as many as possible areas of the statue from almost every part of the body and head. The statue is 1.18 meters high, and thus it was very helpful that the head of the spectrometer could be moved along a meter range vertically. Another feature of the apparatus that has facilitated the analysis is that the head of the spectrometer could be shifted clockwise at various angles. This was required especially at areas with complex geometry, so as the beam direction is always perpendicular to the analyzed surface.

Figure 10. The configuration of the apparatus during the analysis of the nape and left foot. As it can be seen in the photo, the head of the spectrometer changed angle so as to better reach the surface to be analyzed.

7.1.2 Reference Materials

A series of certified reference copper alloys with known chemical compositions were used in this study in order to calibrate the apparatus and to obtain reliable experimental data. The BCR-691 series of copper alloy standards has been issued by the Community Research of the European Union and it consists of five alloys that are all representative of ancient bronze compositions. Each alloy has a different concentration of arsenic, lead, tin and zinc and they are all available as a set of five polished disks with diameter 35 mm and thickness 2mm. These certified alloys provide appropriate matrices particularly with respect to arsenic, which is not found in modern bronzes in significant concentrations (Ingelbrecht, et al., 2001). In order to produce accurate results from these reference bronzes an area of at least $5mm^2$ must be analyzed in order to overcome issues concerning the inhomogeneity of the bronzes caused by the distribution of lead into copper. In bronzes, lead globules are found on the copper grain boundaries, or the surface finishing that result either in partial removal of lead from the inter-granular regions or to a lead smearing across the surface. Before the analysis of the statue, area scans varying from $1mm^2$ to $4mm^2$ were taken on the surface of the disks in order to calibrate the apparatus and verify the results obtained. This range was chosen so as to have a better evaluation of the uncertainties which are introduced when a smaller area than the recommended one is analyzed, since the corrosion free areas on the surface of the statue were not so extended.

Table 1. Nominal, measured and standard deviation values of the reference Cu alloy standards expressed in %w/w. DL indicates that for the particular element the quantification is not possible either due its low content below the detection limits of the analysis or due to interference problems

Elements	BCR$_A$			BCR$_B$		
	Nominal	Measured	SD (%)	Nominal	Measured	SD (%)
Cu	78.73	80	- 1.5	82.7	81	1.8
Zn	6.02	6.0	0.5	14.8	16	-7.4
As	0.19	DL	-	0.099	DL.	-
Sn	7.16	7.2	- 0.8	2.06	2.1	-0.5
Pb	7.9	7.6	4	0.39	DL	-

Table 1. Nominal, measured and standard deviation values of the reference Cu alloy standards expressed in %w/w. DL indicates that for the particular element the quantification is not possible either due its low content below the detection limits of the analysis or due to interference problems

	BCR$_C$			BCR$_D$			BCR$_E$		
	Nominal	Measured	SD (%)	Nominal	Measured	SD (%)	Nominal	Measured	SD (%)
Cu	95.5	89	6.0	80.3	84	- 4.5	92.4	92.8	- 0.4
Zn	0.06	DL	-	0.148	DL	-	0.157	DL	-
As	4.06	5.6	- 23	0.285	DL	-	0.194	0.16	16.5
Sn	0.2	0.27	- 36	10.1	8.7	13.5	7	6.8	2.9
Pb	0.18	DL	-	9.2	7.2	21	0.204	0.22	- 6.4

7.1.3 Description of the analyzed areas

Twenty-three areas in total were chosen to be analyzed with the micro X-ray Fluorescence technique. The areas were selected so as to answer certain analytical questions of the conservators of the Museum before the conservation and the temporary exhibition of the statue.

The analysis of the various areas of the surface of the statue was completed within two days of in-situ measurements. On the first day, analyses were conducted on the areas of the head and upper body, and on the second day on the areas of the lower body and the base of the statue. The conditions of each measurement were adjusted depending on the characteristics of each area such as its morphology, geometry and the information that should be retrieved from it, so as to answer in the best possible way the questions raised. For instance, in order to determine the presence of light elements, unfiltered measurements were selected. In several cases, nearby areas were also measured, so as to be able to compare the results obtained and make appropriate elemental correlations. The main questions raised by the museum conservators were:

1. To identify the chemical composition of the original alloys used to manufacture parts of the bronze statue
2. To confirm initial assumptions made concerning the elemental composition of specific areas such as the inlaid parts (left eyebrow, lips and genitalia)
3. To understand whether areas with a golden to reddish color, a color that resembles the one of a bronze alloy, represent the surface of the original alloy without the presence of corrosion products
4. To confirm or reject the theory that the statue had been cleaned electrochemically with zinc by the end of the 19th century, and
5. To identify specific elements on corroded areas and to suggest possible corrosion products

The following table (no. 2) contains a micro photo of each area analyzed, the label, the conditions of measurements and the analytical questions that arose from this area.
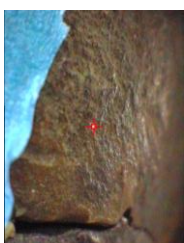
Table 2. Analyzed areas			
Photo	**Name – Area**	**Type of scan / Number of mea/ts / Time per step (s) / Area (mm^2) / Step (mm) / Filtered (F) or Unfiltered (U)**	**Technical observations & analytical questions**
	Ba1 (back of the head / copper plating)	Area scan 10 /20 / 0.16/ 0.10 / F	Confirm that it is a copper plating
	1a1 (back of the neck)	Area scan 30 / 20 / 0.25 / 0.10 / F	Elemental composition & determine whether it is a clean or corroded area
	1a2 (back of the neck)	Area scan 30 / 20 / 0.25/ 0.10 / F	Compare to area 1a1, formation of corrosion products
	1a3 (back of the neck, same area with 1a2)	Area scan 30 / 20/ 0.25 / 0.10/ U	Detect the presence of sulphur
	3a1 (left eyebrow / inlaid)	Area scan 9 / 20 / 0.01 / 0.10 / F	Composition of the inlaid part
	5a1 (nose)	Area scan 12 / 20 / 0.09/ 0.10/ F	Compare to area 1a1, formation of corrosion products

Photo	Name – Area	Type of scan / Number of mea/ts / Time per step (s) / Area (mm^2) / Step (mm) / Filtered (F) or Unfiltered (U)	Technical observations & analytical questions
	5a2 (nose)	Area scan 9 /20 / 0.04 / 0.10 / U	Detection of light elements
	4a1 (lower lip / inlaid)	Area scan 25 / 20 / 0.16/ 0.10 / F	Composition of the inlaid part
	6a1 (upper left chest)	Area scan 12 / 20 / 0.24/ 0.20 / F	Elemental composition, determine whether it is a clean or corroded area
	11a1 (center of the chest)	Area scan 9 / 20 / 0.04 / 0.10 / F	Elemental composition, determine whether it is a clean or corroded area
	11a2 (center of the chest)	Area scan 9 / 20 / 0.04 / 0.10 / U	Detection of light elements
	11a3 (center of the chest)	Area scan 9 / 20 / 0.04 / 0.10 / U	Compare to area 11a2 / Detect any light elements

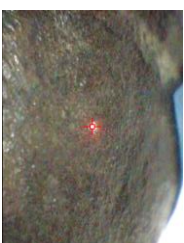| Photo	Name – Area	Type of scan / Number of mea/ts / Time per step (s) / Area (mm^2) / Step (mm) / Filtered (F) or Unfiltered (U)	Technical observations & analytical questions
	11a4 (center of the chest)	Area scan 9 / 20 / 0.04 / 0.10 / F	Compare to area 11a1
	2a1 (back)	Area scan 15 / 20 / 0.08 / 0.10 / F	Elemental composition, determine whether it is a clean or corroded area
	Ma (back / Pb filling)	Area scan 12 / 20 / 0.06 / 0.10 / F	Confirm that it is a lead filling
	12a1 (left testicle)	Area scan 4 / 20 / 0.09 / 0.10 / F	Determine the presence of other elements in these inlaid parts
	12a2 (left testicle)	Area scan 4 / 20 / 0.09 / 0.10 / U	Detection of light elements
	14a1a (tip of the penis)	Area scan 4 / 20 / 0.01 / 0.10 / F	Determine the presence of other elements in these inlaid parts

Photo	Name – Area	Type of scan / Number of mea/ts / Time per step (s) / Area (mm^2) / Step (mm) / Filtered (F) or Unfiltered (U)	Technical observations & analytical questions
	14a2 (tip of the penis)	Area scan 4 / 20 / 0.01 / 0.10 / U	Detection of light elements
	15a1 (pubic hair)	Single spot 20 / U	Detection of light elements
	15a2 (pubic hair)	Single spot 20 / F	Determine the presence of other elements in these inlaid parts
	8a1 (right thigh)	Area scan 12 / 20 / 0.09 / 0.10 / F	Elemental composition, determine whether it is a clean or corroded area
	8a2 (right thigh)	Area scan 12 / 20 / 0.09 / 0.10 / F	Elemental composition, determine whether it is a clean or corroded area
	8a3 (right thigh)	Area scan 12 / 20 / 0.09 / 0.10 / F	Formation of corrosion products, compare to area 8a1 or 8a2
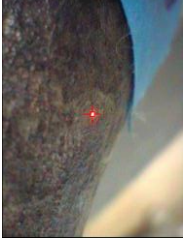
Photo	Name – Area	Type of scan / Number of mea/ts / Time per step (s) / Area (mm^2) / Step (mm) / Filtered (F) or Unfiltered (U)	Technical observations & analytical questions
	8a4 (right thigh)	Area scan 12 / 50 / 0.09 / 0.10 / U	Detection of light elements
	8a5 (right thigh / white area)	Area scan 12 / 50 / 0.06 / 0.10 / U	Detection of light elements
	8a6 (right thigh / white area)	Area scan 12 / 20 / 0.06 / 0.10 / F	Formation of corrosion products, compare to area 8a1 or 8a2
	13a1 (axis of support / right leg)	Area scan 12 / 20 / 0.24 / 0.20 / F	Confirm that the support axis is a brass
	7a1a (left leg)	Area scan 4 / 20 / 0.01 / 0.10 / F	Confirm that it is a copper plating area
	7a2 (left leg	Area scan 4 / 20 / 0.01 / 0.10 / F	Confirm that it is a copper plating area Compare to area 7a1a

Photo	Name – Area	Type of scan / Number of mea/ts / Time per step (s) / Area (mm^2) / Step (mm) / Filtered (F) or Unfiltered (U)	Technical observations & analytical questions
	Aa1 (copper plating	Area scan 9 / 20 / 0.01 / 0.10 / F	Confirm that it is a copper plating
	9a1	Area scan 12 / 20 / 0.06 / 0.10 / F	Compare to area 8a2, formation of corrosion products
	9a2	Area scan 25 / 20 / 0.16 / 0.10 / F	Compare to area 8a2, formation of corrosion products
	9a3	Area scan 12 / 20 / 0.09 / 0.10 / F	Compare to area 8a2, formation of corrosion products
	9a4	Area scan 12 / 20 / 0.09 / 0.10 / U	Detection of light elements
	10a1 (base)	Area scan 9 / 20 / 0.09 / 0.10 / F	Determine the presence of different elements with respect to elements detected from the main statue.

7.2 Data analysis

7.2.1 Qualitative & quantitative analysis

For the analysis of the accumulated spectra from the scan measurements the program QXAS-AXIL was used (Kregsamer, 2009). Due to the interference of the AsKα with PbLα as well as of the CuKβ with ZnKα characteristic X-rays, the PbLβ and ZnKβ lines were used and the assessment of the results obtained was made by using the BCR series.

The quantification procedure was carried out by means of an in-house developed software based on the fundamental parameters approach which is based on the theoretical relationship between measured X-ray intensities and the concentration of the elements in the sample. To determine the X-ray lens transmission efficiency and instrumental geometrical factor a set of pure single element or compound targets were used (Kantarelou & Karydas, 2016). The quantification model developed was tested during an inter-comparison exercise organized by the Getty Museum (Heginbotham, et al., 2010).

7.2.2 The use of SnK/L relative intensities

The mean elemental intensities of SnLα, CuKα, PbLα and SnKα obtained by means of an area scan over a selected area with specific coloration were calculated. The elemental intensities have been normalized to the corresponding ones measured on a pre-cleaned area (whenever such an action was allowed by the museum conservator who have undertaken this action). Therefore, the increase or decrease of the elemental intensity compared to the clean area, can provide a first semi-quantitative information on the elemental content of the corroded area. Generally, if the relative intensity for a particular element is increased or at least remains constant, then certainly this element is a constituent of a corrosion layer. Of course, it should also be stressed that any relative decrease does not necessarily suggest the absence of the particular element from the corroded surface. The presence of carbonates, sulphates and other anions in a corrosion product may reduce significantly its elemental abundance within the compound and most probably its elemental intensity as well. Furthermore, the comparison of the relative intensities among the Lα and Kα characteristic X-rays of the same element (for example Sn) can reveal its selective

surface enrichment (the relative Lα/Kα intensity increases) or absence (the relative Lα/Kα intensity decreases) from the surface layers. This ratio (L/K) is a very sensitive parameter that changes significantly in the presence of a corrosion layer. A lower value of the ratio (L/K) than the one obtained from the raw bronze metal may indicate the presence of copper-based corrosion products, whereas a higher value the presence of a tin based compound (Kantarelou, et al., 2007). The graphic representation of these intensities can be helpful in order to make comparisons among the analyzed areas, while it also allows to observe elemental correlations, and possibly associate the presence of certain elements with a certain corrosion product

In the paper *"In situ scanning micro-XRF analyses of gilded bronze figurines at the National Museum of Damascus"* V. Kantarelou et al., developed a quantification criterion known as the G_{Sn} factor for the identification of corroded areas in binary copper-tin alloys containing tin up to 15%, which is derived from the use of the relative intensities of SnKα/SnLα that was discussed above. The ratio of SnKα/SnLα X-ray intensities normalized to the respective ratio obtained for an alloy with 10% Sn concentration is expressed by the so-called G_{Sn} factor which takes values in the range from 0.89 to 1.17 (fig. 11). This particular range of G_{Sn} values is indicative of an uncorroded alloy surface, while if $G_{Sn} > 1.17$ the presence of a copper corrosion product can be suggested. In the case that $G_{Sn} < 0.89$ the presence of a tin corrosion product is more likely.
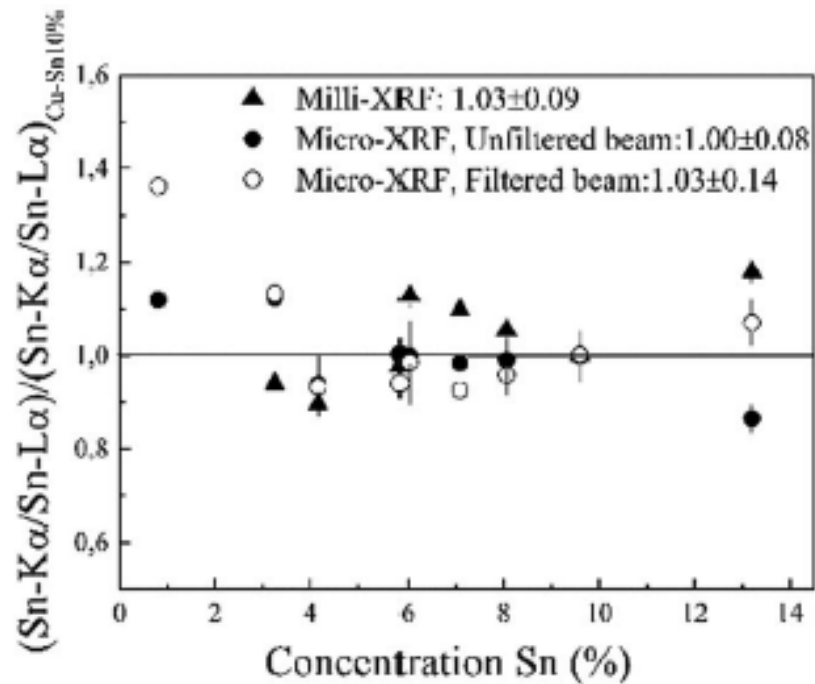
Figure 11. *The variation of the SnKα to SnLα normalized ratio (with respect to the value obtained from a binary Cu90%–Sn10% alloy), as a function of the Sn concentration measured from a set of reference binary Cu–Sn bronze alloys. The measurements were performed using two portable XRF spectrometers and three different experimental conditions. (Kantarelou, et al., 2015, p. 1791)*

For the determination of the G_{Sn} factor two different set of reference materials and two different spectrometers were used. The application of three different excitation modes was made by means of (a) micro-XRF analysis with an unfiltered exciting beam (with 50 kV as an operational voltage), (b) micro-XRF analysis with a filtered exciting beam (50 kV) and (c) milli-XRF analysis using a filtered (40 kV) exciting radiation for Sn-Ka analysis and an unfiltered one (15 kV) for Sn-La analysis.

8. Results and Discussion

8.1 Elemental composition

The final qualitative and quantitative results can be found in tables 7 and 8 respectively. Out of the 23 areas that were analyzed in total, quantitative analysis was conducted for the facial inlaid parts (chapter 8.3) and for the areas with copper platings (chapter 8.5) in order to confirm that they were made out of pure copper. For the remaining areas, the G_{Sn} factor which was thoroughly discussed in sub-chapter 7.2.2 was calculated so as to show which ones are the most representative of the original alloy composition.

Figure 12 is the graphic representation of the value of G_{Sn} factor for every analyzed area. As it is observed the areas that fall within the acceptable range of 1.03 ± 0.14 are: 5a1, 11a1, 8a1 and 7a2 and so they can be considered to represent better the original alloy composition.
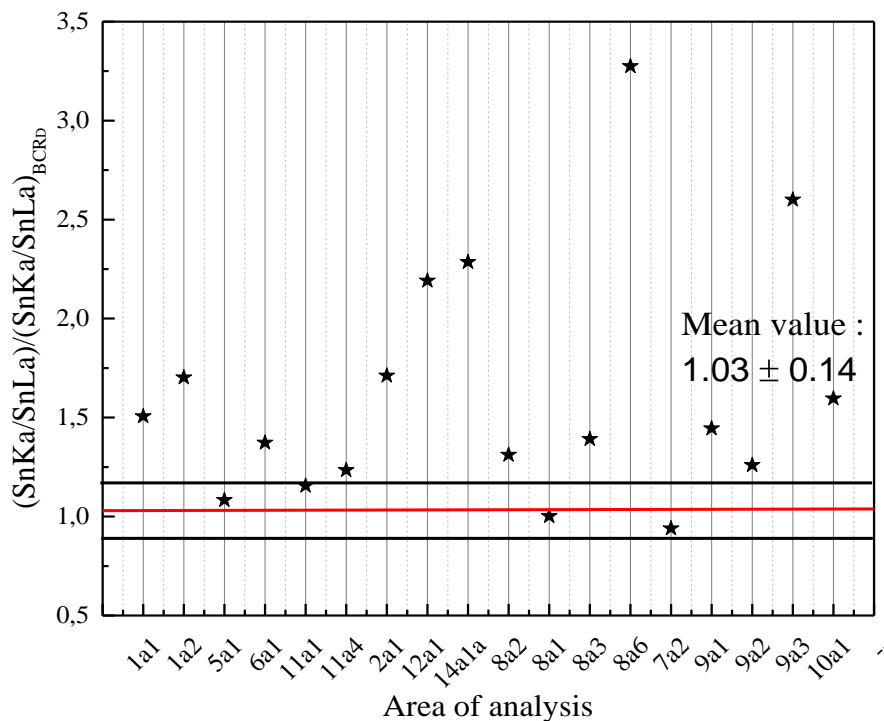
Figure 12. Graphic representation of the G_{Sn} factor of every analyzed area. The two black lines represent the acceptable range of the G_{Sn} factor and all the areas in presented in stars.

Figure 13. *Areas 5a1 (nose), 11a1 (center of the chest), 8a1 (right thigh) and 7a2 (left leg)*

Another criterion, the normalization factor for the closure of the sum of the detected elemental concentrations (ideally equal to 1)**,** was also used to further narrow the number of areas that can be considered as the most representative, since a value of the normalization factor less than 0.95 and higher than 1.05 can serve as an additional indication that a corrosion layer might exist at the surface of the metal. Figure 14 is the graphic representation of the G_{Sn} factor as a function of the normalization factor and it can be observed that areas 11a1 and 5a1 provide a non-acceptable value of 0.84 and 1.5 respectively, in comparison to areas 8a1 and 7a2 that have an acceptable normalization factor of 0.95.
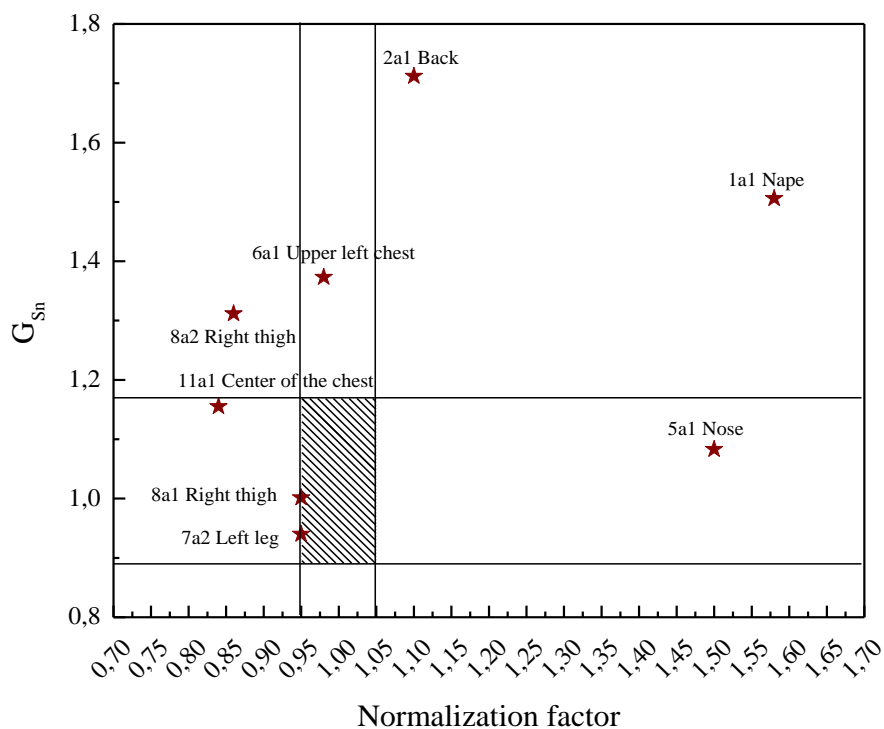
Figure 14. The G_{Sn} factor as a function of the normalization factor, as it is deduced from the quantification process, provides a more enhanced criterion to better identify corrosion-free areas. The box filled with the line pattern represents the acceptable Gsn and normalization factor ranges.

The following table (no. 3) contains the elemental composition in %w/w of area 8a1 and 7a2 that were determined as the most representative of all the analyzed areas from the graphic representation of the G_{Sn} factor as a function of the normalization factor.

Table 3. The elemental composition of the Bronze statue of Poseidon of Livadostra in % w/w (with standard deviation in % of the characteristic X-ray intensities during area scans)							
Elements	**Mn**	**Fe**	**Cu**	**Zn**	**As**	**Sn**	**Pb**
Areas							
8a1	0.025 D.L.	0.17 (31.4)	86.9 (15.1)	0.15 (31.9)	0.157 (35.6)	11.7 (59.5)	0.875 (46.6)
7a2	0.025 D.L.	0.165 (21)	88.5 (13.5)	0.3 (36.8)	0.106 (29.6)	9.67 (53.1)	1.28 (60.6)

8.2 Comparison to other statues and statuettes

In order to be able to verify that the concentrations of the various elements that were determined in the statue of Poseidon, correspond to the concentrations of other statues that originate from the archaic and classical years, a comparative study was made with bibliographical data. Because there are no other surviving statues from this transitional period from the archaic to classical years, the present results were compared with those reported in the study by Paul T. Craddock under the title: "The Composition of the Copper Alloys used by the Greek, Etruscan and Roman Civilizations part 2. The Archaic, Classical and Hellenistic Greeks". In this study published in 1977, Craddock shared the results of the analysis that were conducted on more than 500 bronze statuettes, decorative and functional bronzes.

For the purpose of comparison, only the concentration of the sixty-one archaic statuettes and of thirty-two belonging to the classical period will be used and will be presented in the form of a box chart. In the box chart the smaller lower and upper line present the minimum and maximum value of the sum respectively. The lower line of the box represents the first quartile and the upper line the third quartile. The small square inside the box represents the mean value and the horizontal line located also inside the box is the median. The small stars located on the lower and upper side of the vertical line represent the outliers.

The average concentration of copper obtained from the statue of Poseidon as shown in fig. 15 falls within the range of both the archaic and classical years, but seems to be closer to the average concentration of the classical years.
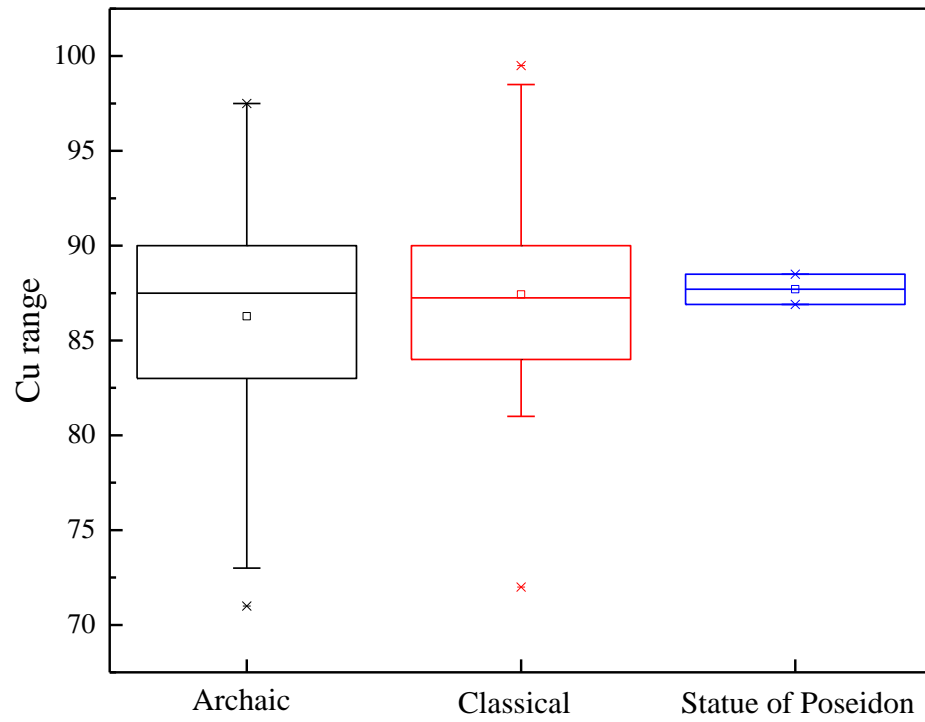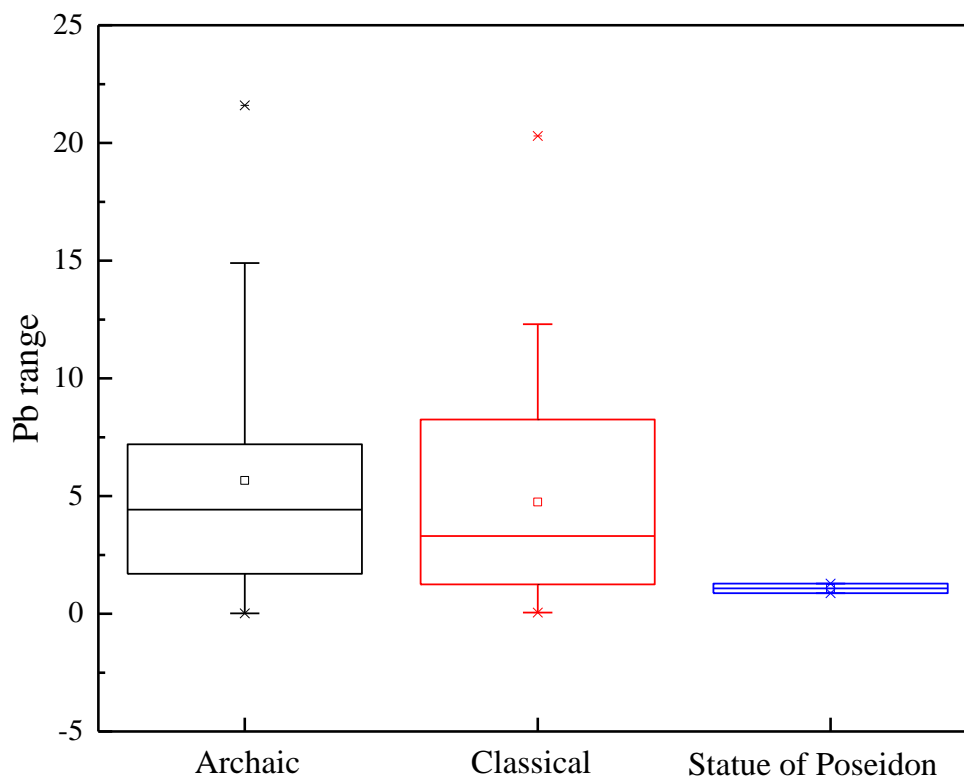

Figure 15*. Box chart presenting the range of Cu concentration in the archaic and classical eras and the bronze statue of Poseidon*
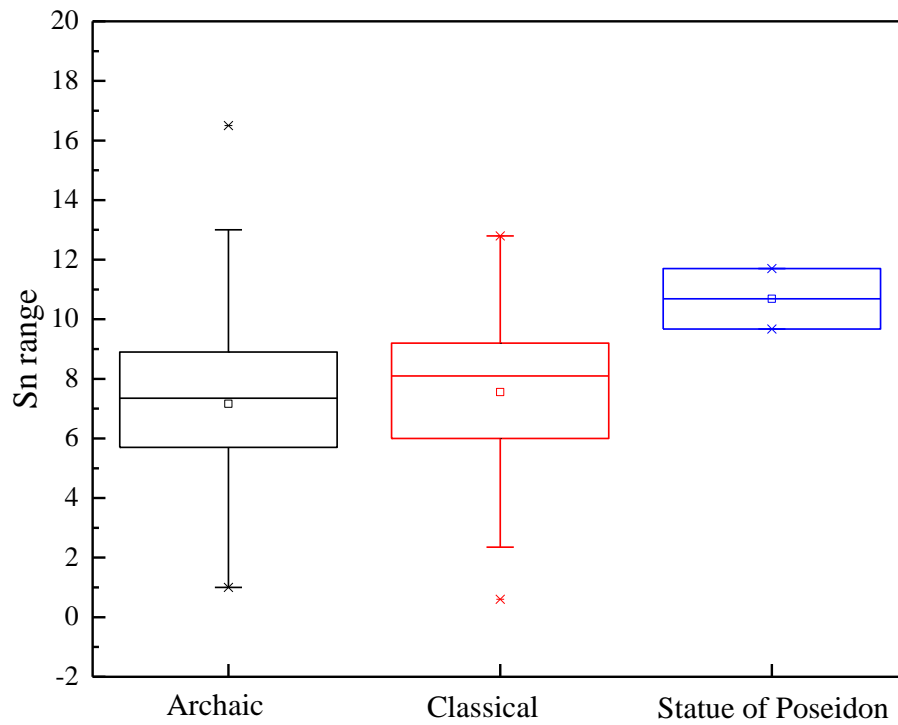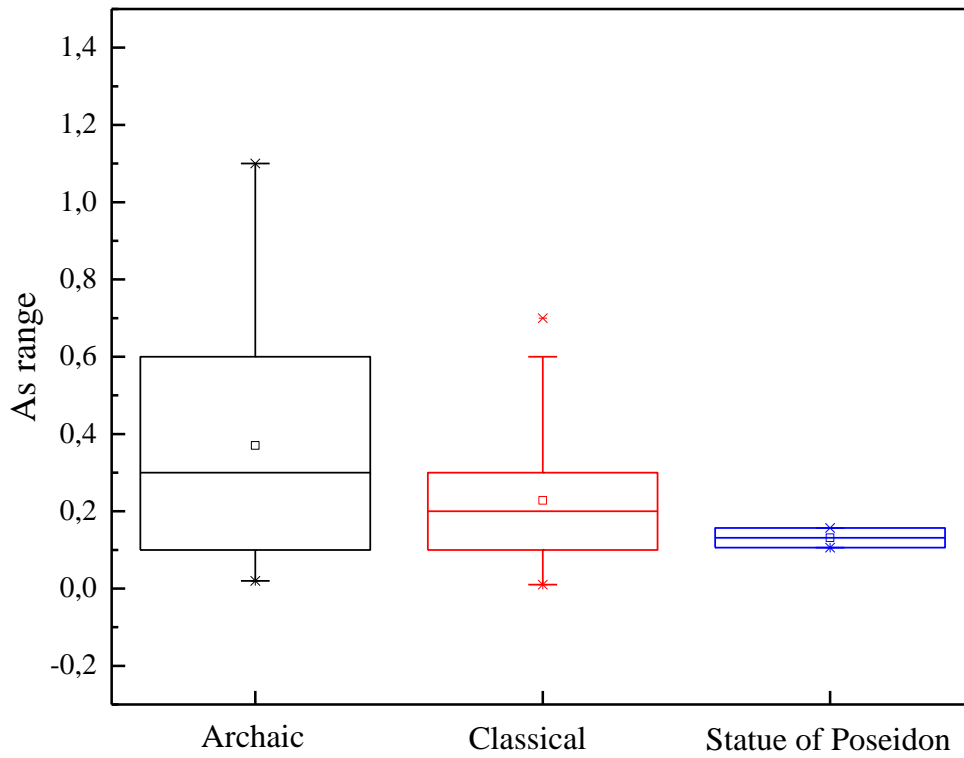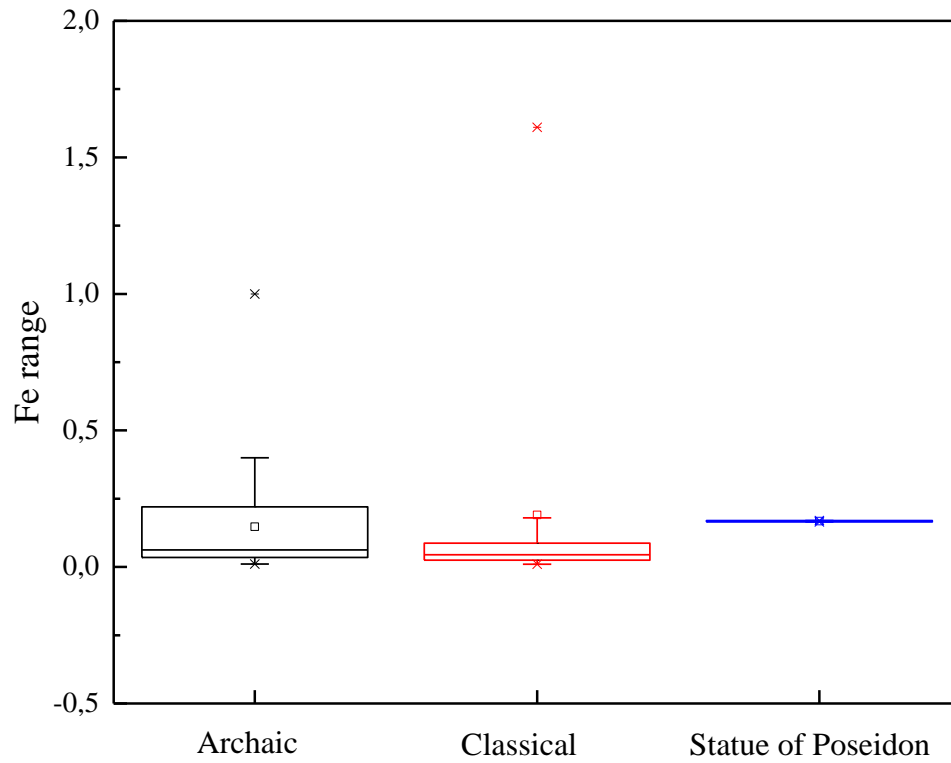
Figure 16*. Box chart presenting the range of Sn concentration in the archaic and classical eras and the bronze statue of Poseidon*

As it can be seen in figure 16, the range of tin concentration in the archaic and classical years remains fairly constant with great variations being observed among bronze statuettes that were manufactured during the same era. Tin concentration of the statue of Poseidon falls within the range of both the archaic and classical years but no attribution to a specific era can be made.

The mean concentration of lead in the statue of Poseidon as shown in figure 17 is less than those of the archaic and classical years, but within the respective standard deviations, thus it cannot be determined at which period the lead content of Poseidon statue is closer to. It is also important to mention that even if the chronological classification of the statue had not been done based on its technical characteristics, or there was no clue of the exact location that the statue was found, the concentration of lead would have played a principal role in order to attribute the statue to a specific period.

***Figure 17**. Box chart presenting the range of Pb concentration in the archaic and classical eras and the bronze statue of Poseidon.*

Figure 18. Box chart presenting the range of As concentration in the archaic and classical eras and the bronze statue of Poseidon

The mean arsenic concentration of the statue of Poseidon is less than the ones of the archaic and classical eras. The range though of the classical years is lower than the archaic ones and thus the arsenic content of the statue seems to be closer to the classical years.

On the other hand, the mean concentration of iron in the statue of Poseidon exceeds the mean iron concentration of the classical years and seems to be closer to the archaic ones.

Figure 19. *Box chart presenting the range of Fe concentration in the archaic and classical eras and the bronze statue of Poseidon*

In figure 20, it is observed that the mean concentration of zinc determined in the statue of Poseidon is closer to the the mean concentration of the classical years, but since the standard deviation of the archaic era is high, it cannot be precisely determined in which era the zinc content of Poseidon is closer to.
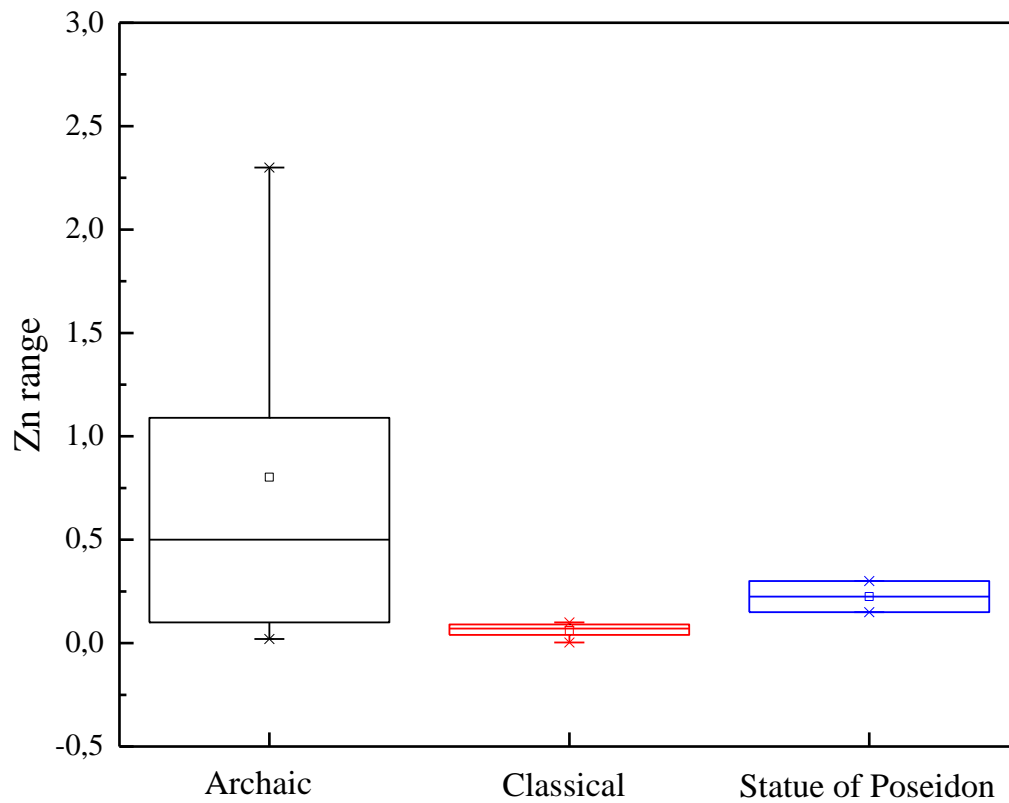
Figure 20. Box chart presenting the range of Zn concentration in the archaic and classical eras and the bronze statue of Poseidon

Other analyses on ancient Greek bronze statues that can be found on the table below present similar concentrations of copper, tin, zinc and lead in relation to the ones that were determined in Poseidon.

Table 4. The elemental composition of other known statues of the archaic and classical eras							
Statue	**Date**	**Elemental composition in % w/w**					
		Cu	**Sn**	**Pb**	**Zn**	**Fe**	**As**
Apollo of Piraeus[3]	525	87	10	-	-	-	-
Chatsworth Head (of Apollo)[4]	460	87.5	10.4	0.02	0.01	0.02	0.10
Chatsworth Leg (of Apollo)[5]		91.5	8.9	0.570	0.03	0.37	Traces
Riace bronze A-Body[6]	460-450	88.8	10.75	0.12	-	0.13	-
Riace bronze A-Head		87.35	12.41	0.062	0.004	0.035	-
Riace bronze B-Body	460-450	90.08	9.26	0.155	0.01	0.16	-
Riace bronze B-Head		85.94	13.5	0.233	0.005	0.13	-

---

[3] (Varoufakis, 1965)
[4] The head and the leg of the statue contain also small amounts of Ag, Au, Sb, Ni and Co.
[5] (Craddock , 1977)
[6] (Buccolieri, et al., 2015) pp. 102

8.3 Inlaid parts

The results obtained by the XRF analysis were able to confirm the observation made by the laboratory personnel during the close visual observation concerning the inlaid parts of the face. The remaining left eyebrow and the lips, consist of pure copper with a concentration of 98.3% and 98% respectively, something that was expected since most inlaid facial parts of the statues of that era were made out of copper for aesthetic reasons.

3a1- Left eyebrow   4a1- Lower lip
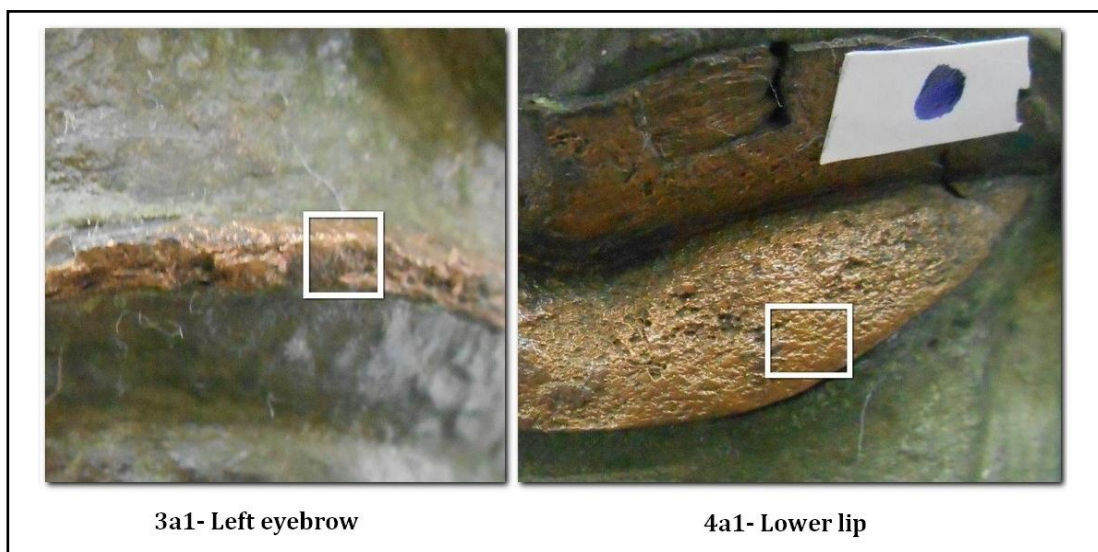
Figure 21. *Close photo of the inlaid facial parts*

Table 5. The elemental composition of the inlaid parts in % w/w (with standard deviation % of the characteristic X-ray intensities during area scans)							
Elements	**Mn**	**Fe**	**Cu**	**Zn**	**As**	**Sn**	**Pb**
Areas							
3a1	0.015 D.L.	0.167 (28.5)	98.3 (53.2)	0.261 (48)	0.316 (58.8)	0.566 (45.3)	0.326 (44.2)
4a1	0.015 D.L.	0.105 (34.5)	98 (29.5)	0.285 (54.7)	0.493 (35.2)	1.014 (38.1)	0.083 (35.7)
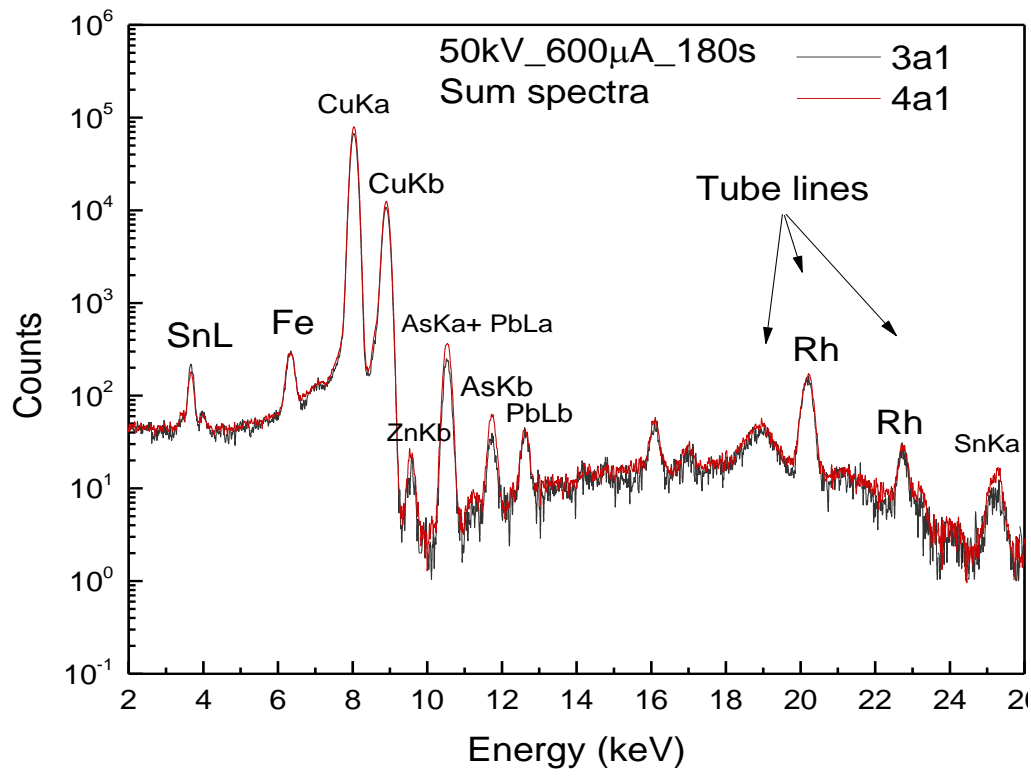
Figure 22. *Sum spectra acquired from the facial inlaid parts*

8.4 Lead filling

The XRF analysis made it also possible to determine that the filling (area Ma1) that was used in a previous conservation treatment in order to cover the crack at the back of the statue was indeed made out of lead as shown in the following spectrum.
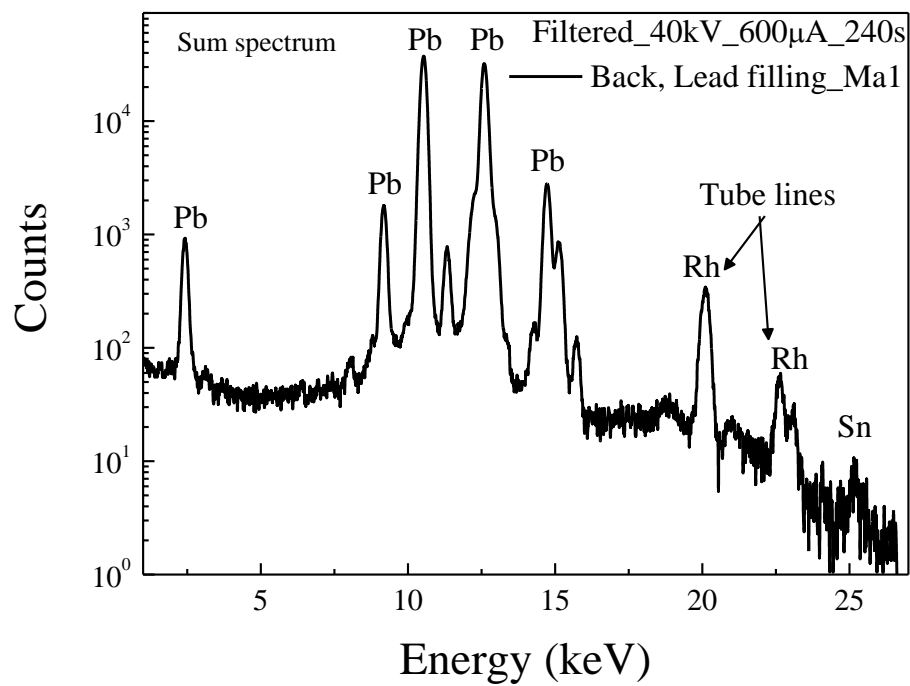
Figure 23. Sum spectrum acquired from the lead filling that is located at the back of the statue

8.5 Corrosion products
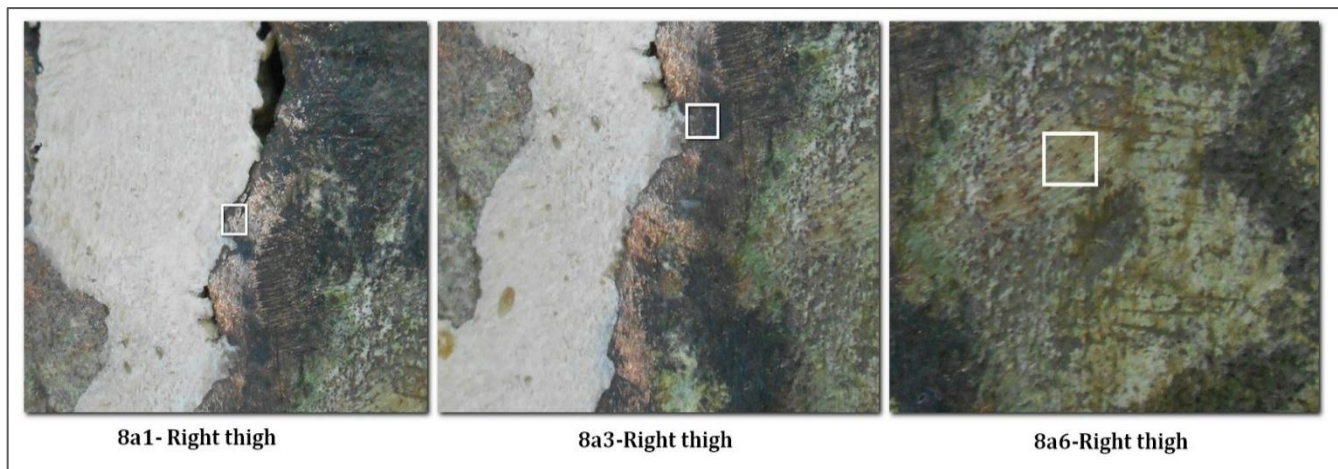
Figure 24. *Close photo of areas 8a1, 8a3 and 8a6*

The mean relative intensities of CuKα, SnKα, SnLα and PbLα of certain selected areas to a clean area that was determined by the Gsn factor as a function of the normalization factor were calculated and a graphic representation was created so as to observe their course and suggest possible corrosion products.
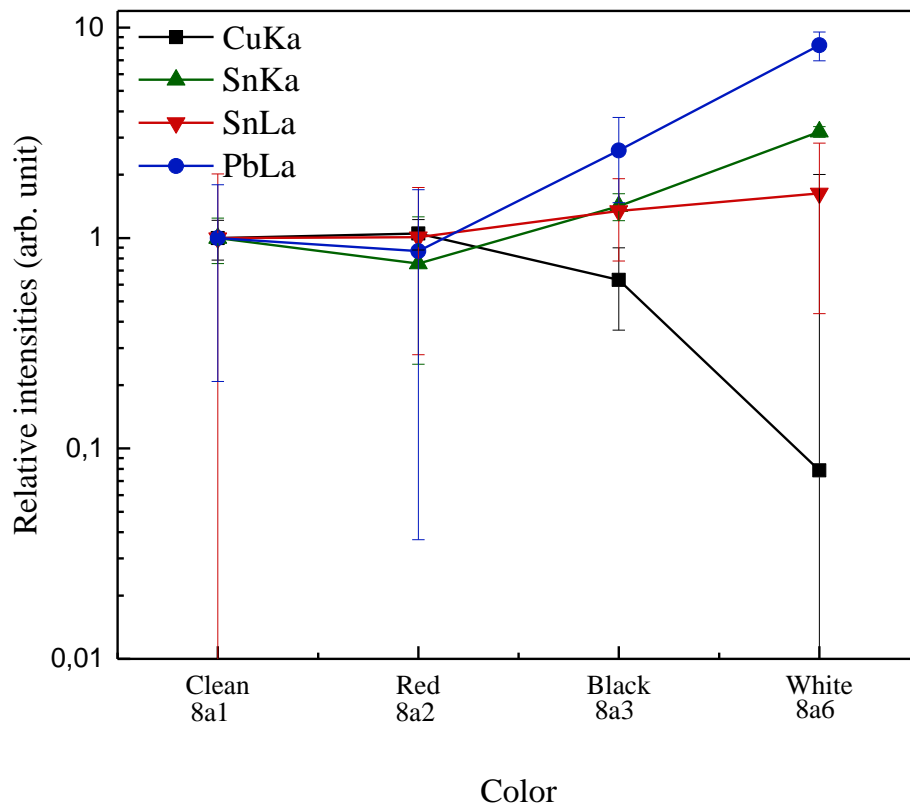
***Figure 25**. Mean relative intensities of certain selected areas*

In area 8a2 it can be observed that there is a decrease in SnKα and PbLα and a slight increase in SnLα and CuKα, but with the standard deviations of the relative intensities of all the characteristic X-rays, it is hard to suggest possible corrosion products. In the black area (8a3) a decrease in the intensity of CuKα and an increase in SnLα, SnKα and PbLα can be observed, an indication of a lead corrosion product. In the white area (8a6) there is a decrease in the intensity of CuKα and an increase in SnKα and PbLα. This is an indication that a lead based corrosion product together with a tin based corrosion product could be located in the area.

From the graphic representation of the GSn factor (fig.11) it is known that for all the areas that fall below the value of 0.89 this in an indication of the presence of a tin enrichment in the surface and this is attributed to the fact that the SnL lines require a lower energy threshold in order to get excited than the SnK lines. This

means that a SnKα/SnLα ratio lower than the one obtained from a clean surface is an indication of a tin enriched surface.

For instance, the values for areas 1a1 and 1a2 are above 1.17, so it is an indication of a copper or lead enrichment on the surface. From the qualitative results obtained from these areas, it can be seen that there is a decrease in their counts of copper and an increase in their counts of tin and lead in comparison to the counts of the same elements in area 8a1 (appendix table I). This is an indication that even though there can be a tin enrichment in the surface, lead corrosion products overlap those of tin. The same observation can be also made when comparing area 6a1 to area 8a1, where the counts of copper reduce in half, the counts of tin almost double and those of lead almost triple. The comparison of area 8a6 to area 8a1 is also a strong indication that when there is an increase in PbLα, SnKα and SnLα (fig. 25), in the graphic representation of the G_{Sn} factor the lead enrichment overlaps the tin corrosion products.

Moreover, when comparing the suggested corrosion products derived from the mean relative intensities of areas 8a2, 8a3 and 8a6 (fig. 25), to their location at the graphic representation of the G_{Sn} factor (fig. 11), it can be observed that the suggested corrosion products are in accordance with the G_{Sn} factor.

An interesting pattern was observed when comparing area 8a1 to areas that are located near cracks. It can be observed that areas 6a1, 2a1, 8a3 and 7a1a present an increase in their lead counts, an indication that all the cracks of the statue may have once been filled with lead (chapter 8.4) and that an extensive phenomenon of contamination may have taken place.

8.6 Copper platings

Areas Ba1 and Aa1 were confirmed to be copper platings (a product of copper reduction process), because the concentration of copper reaches up to 99.7% and 98.9% in these areas respectively. With the XRF analysis it was also possible to classify area 7a1a also as a copper plating, because of its high copper content that reaches up to 96.6%, something that by the macroscopic observation was not possible.
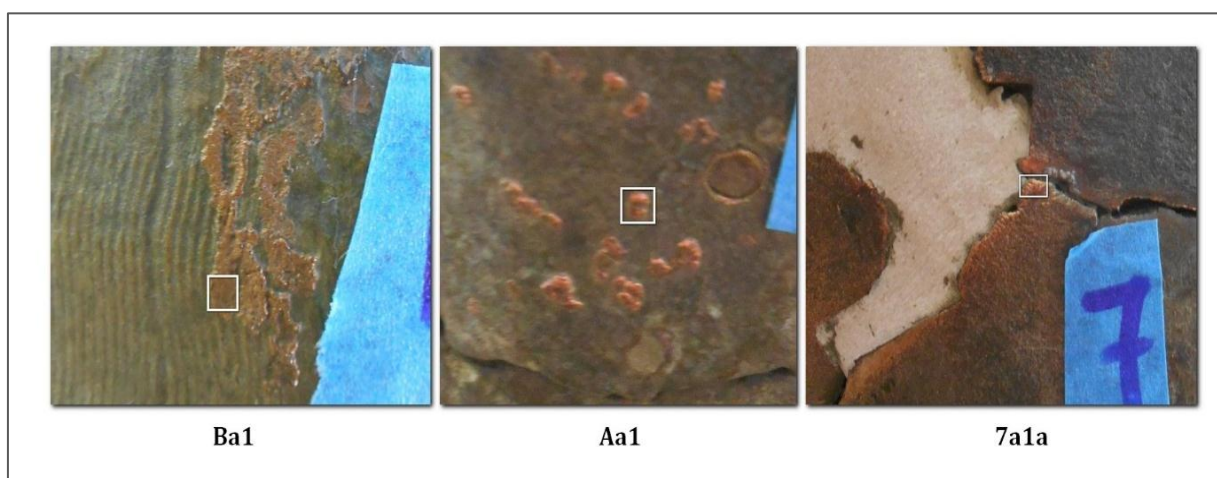

Figure 26. Example of copper platings areas Ba1 & Aa1

Table 6. The elemental composition of the copper platings in % w/w (with standard deviation % of the characteristic X-ray intensities during area scans)							
Elements	**Mn**	**Fe**	**Cu**	**Zn**	**As**	**Sn**	**Pb**
Areas							
Aa1	0.016 D.L.	0.018 (57)	99.7 (35)	0.223 (37.4)	0.037 (44.5)	nd	0.04 (41.9)
Ba1	0.016 D.L	0.0091 (30)	98.9 (9.12)	0.018 (37.5)	0.013 (40.8)	0.884 (36.2)	0.0165 (41.9)

8.7 Light element analysis

During the analyses, several unfiltered measurements were taken in order to detect light elements. No light elements such as chloride or sulphur were detected, an indication that any corrosion products attributed to the marine environment had been successfully removed, at least from the areas that were analyzed, during previous conservation treatments. Moreover, the fact that no sulphur was detected is a valuable clue that gives information about the mining and extraction techniques of the metals that were used and especially for copper. The absence of sulphur could be an indication of a successful roasting stage during the manufacturing of the statue.
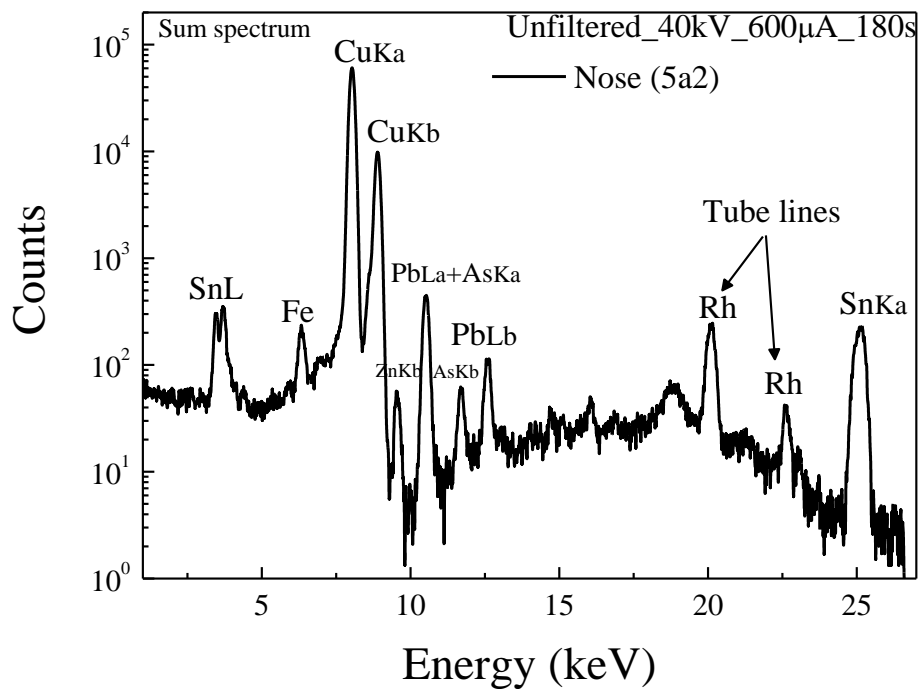
Figure 27. *Sum spectrum acquired from the area of the nose (5a2)*
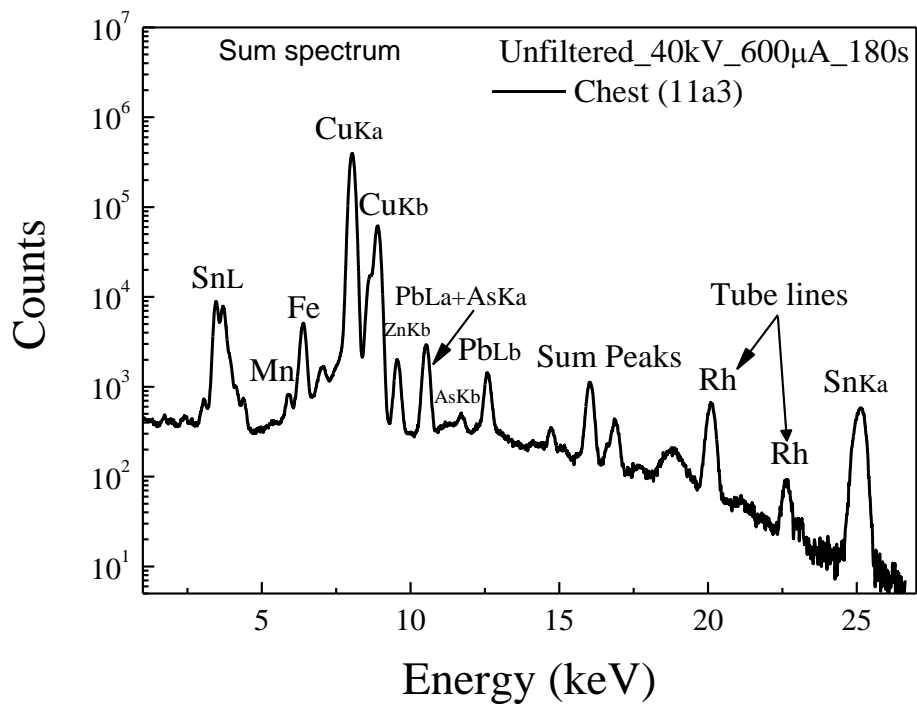
Figure 28. Sum spectrum acquired from the area of the chest (11a3)
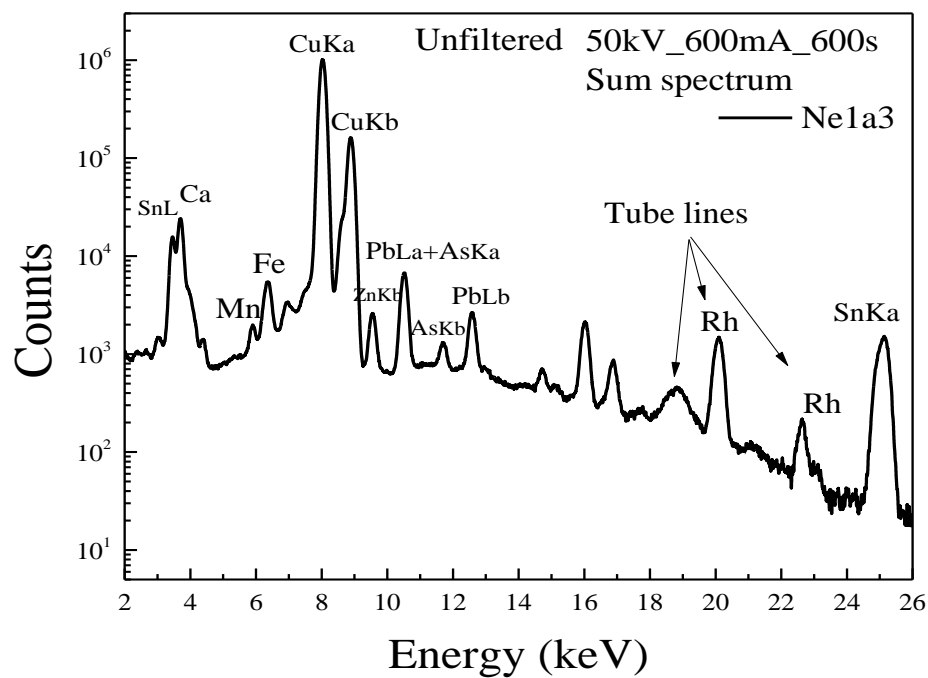
Figure 29. Sum spectrum acquired from the area of the nape (1a3) acquired from the area of the nape

8.8 Electrochemical cleaning with zinc

One of the major questions was whether the bronze statue of Poseidon had been cleaned electrochemically with zinc at the end of the 19th century, a procedure that would alter the surface of the statue by increasing its zinc concentration. In order to be able to answer this question a thorough investigation had to be made in every area by comparing its counts in zinc not only to the rest of the areas, but also in relation to the other trace elements that were detected in the alloy. As shown in the first graph bellow there is a variance from area to area in the counts of zinc. The part of the body that presents the less variance is the head, but generally throughout the surface of the statue variations in the counts are observed not only among nearby areas, but also in the counts of other elements such as iron, arsenic and lead.
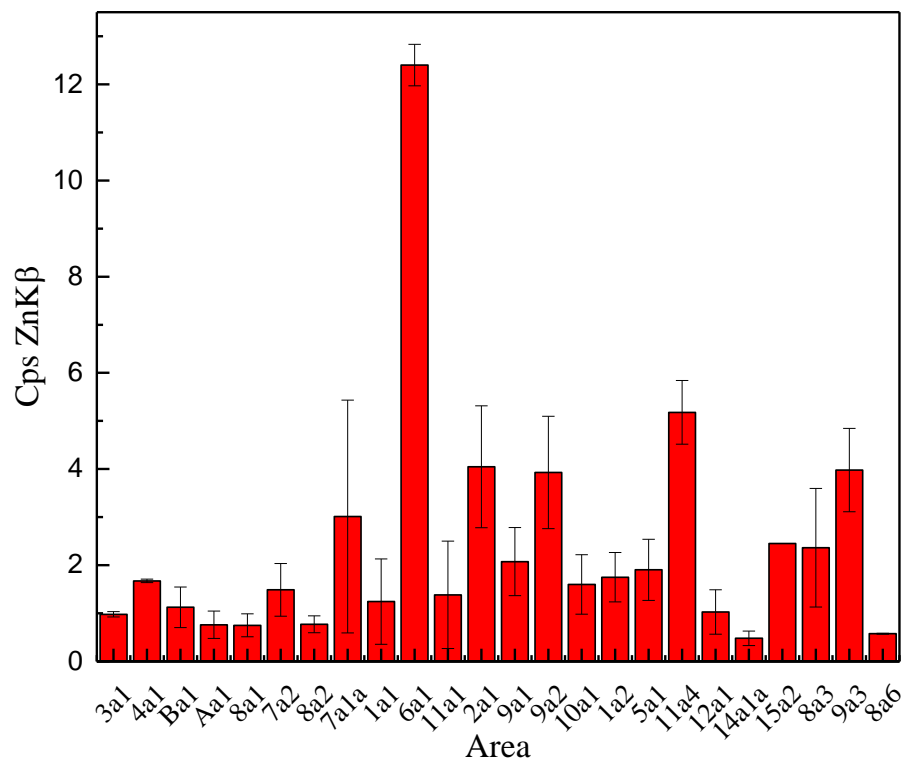
Figure 30. ZnKβ counts per second & standard deviation in every analyzed area
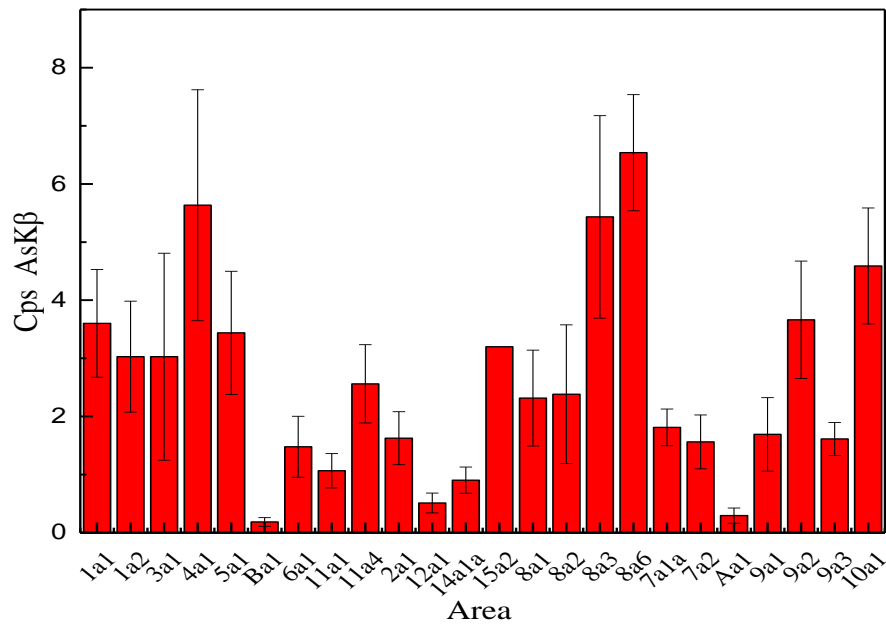
Figure 31*. AsKβ counts per second & standard deviation in every analyzed area*
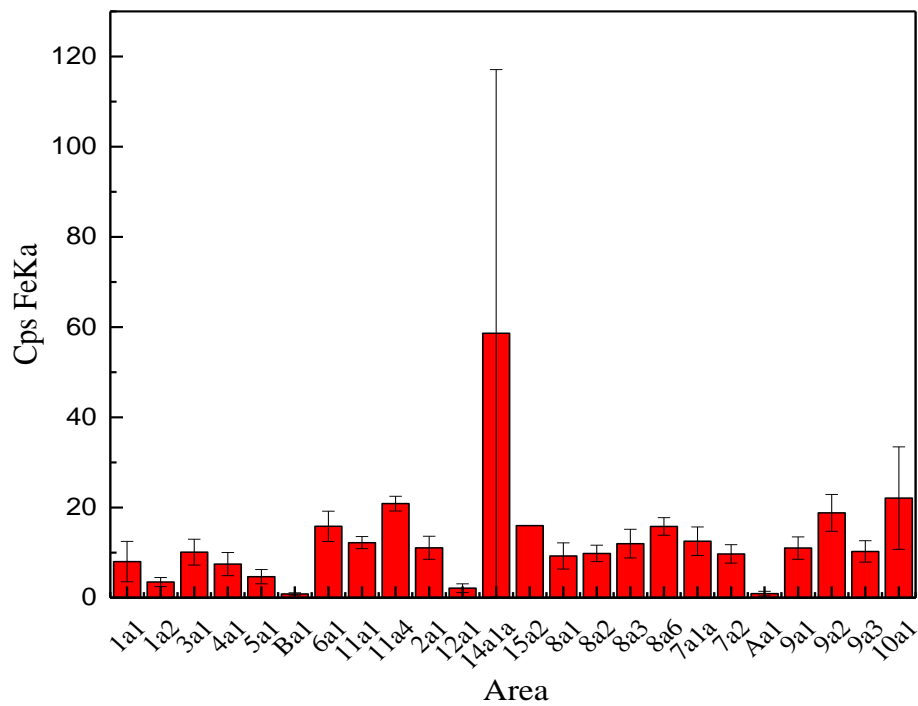
Figure 32*. FeKα counts per second & standard deviation in every analyzed area*
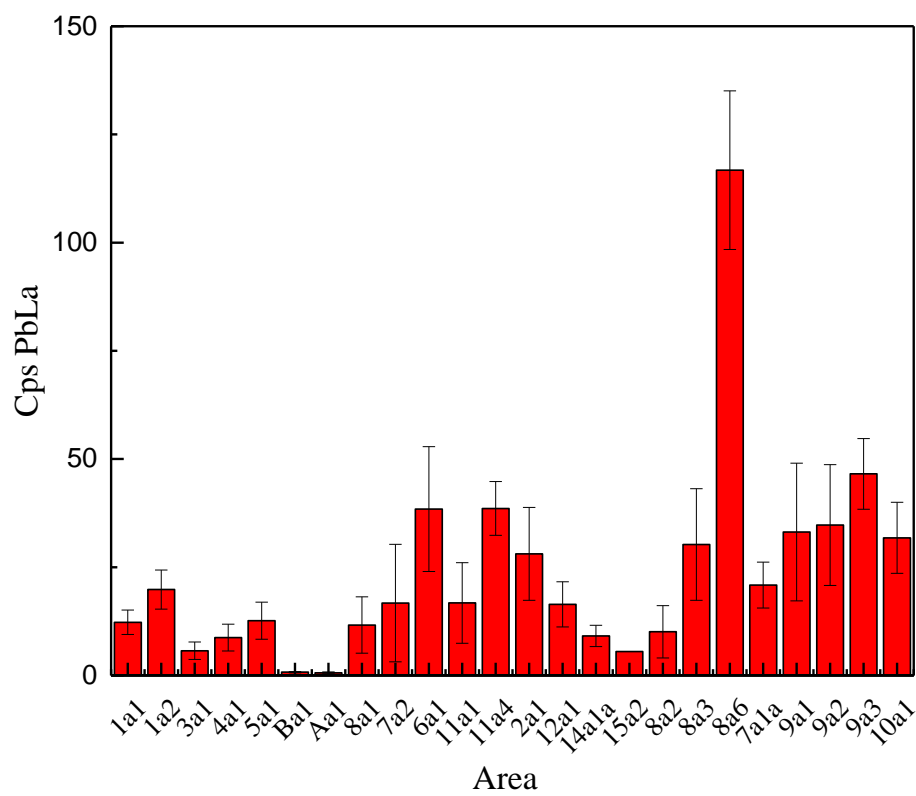
Figure 33. *PbLα counts per second & standard deviation in every analyzed area*

9. Conclusions

The non-destructive, in-situ micro-XRF analysis of the statue of Poseidon of Livadostra and the applied analytical methodology helped to identify that the statue was made by a binary alloy with 87.7 % copper and 10.7% tin, whereas minor amounts of lead and traces of other elements such as manganese, iron, zinc and arsenic are also included in the bronze metal. Moreover, it was confirmed that the inlaid facial parts, such as the left eyebrow and lips consist of pure copper with a concentration of 98.3% and 98%, respectively.

The present study has also discovered that in a previous conservation treatment a lead filling was used for the coverage of the various cracks that has subsequently caused an excessive contamination effect in the areas located near those filled cracks. From the comparison of the mean relative CuKα, SnKα, SnLα and PbLα characteristic X-ray intensities measured from various corroded areas versus their respective value obtained from a clean micro-area of the bronze alloy, it was possible to identify that the surface of the statue is covered with various copper, tin and lead based corrosion products.

The elemental composition of the Poseidon statue has been compared with the ones reported for other statues that date back to the archaic and classical years. The comparison showed no essential differences with respect to the major, minor and trace elements detected in the bronze statue of Poseidon of Livadostra. Concerning the question posed, if an electrochemical cleaning with zinc was applied, no strong evidence that could support such a hypothesis was found.

10.   References

Alberghina, M. F. et al., 2011. Integrated analytical methodologies for the study of corrosion process in archaeological bronzes. *Spectrochima Acta Part B*, pp. 129-137.

Aravatinos, V., Konency, A. & Marchese, R., 2003. Plataiai in Boiotia: A Preliminary Report of the 1996-2001 Campaigns. *Hesperia: The Journal of the American School of Classical Studies at Athens*, 72(3), pp. 281-320.

Buccolieri, G. et al., 2015. Portable EDXRF investigation of the patinas on the Riace Bronzes. *Nuclear Instruments and Methods in Physics Research* , B(343), pp. 101-109.

Caley, E., 1951. Chemical Investigations of Two Ancient Bronze Statuettes Found in Greece. *Ohio Journal of Science*, 51(1), pp. 6-12.

Craddock , P., 1977. The Composition of the Copper Alloys used by the Greek, Etruscan and Roman Civilizations: 2. The Archaic, Classical and Hellenistic Greeks. *Journal of Archaeological Science*, pp. 103-123.

Craddock, P., 2009. *Scientific investigation of copies, fakes and forgeries.* Oxford: Butterworth-Heinemann.

Craddock, P. & Meeks, N., 1987. Iron in Ancient Copper. *Archaeometry*, 29(2), pp. 187-204.

Ferretti, M., 2014. The investigation of ancient metal artefacts by portable X-ray fluorescence devices. *Journal of Atomic Spectroscopy*, pp. 1753-1767.

Gianoncelli, A. & Kourousias, G., 2007. Limitations of portable XRF implementations in evaluating depth information: an archaeometric perspective. *Journal of Applied Physics*, pp. 857-863.

Haynes, D., 1992. *The Technique of Greek Bronze Statuary.* Mainz am Rhein: Verlag Phillip von Zabern.

Heginbotham, A. et al., 2010. An evaluation of inter-laboratory reproducibility for quantitative XRF of historic copper alloys. *Proceedings of the interim meeting of the ICOM-CC Metal working group*, pp. 244-255.

Houser, C., 1983. *Greek Monumental Bronze Sculpture.* London: Thames & Hudson .

Ingelbrecht, C., Adriaens, A. & Maier, E. A., 2001. *The certification of arsenic, lead, tin and zinc (mass fractions) in five copper alloys BCR-691,* Luxembourg: European Commission.

Janssens, K. et al., 2000. Use of microscopic XRF for non-destructive analysis in art and archaeometry. *X-ray Spectrometry*, January, pp. 73-91.

Kaltsas, N., 2007. *The National Archaeological Museum.* s.l.:John Latsis Public Benefit Foundation.

Kantarelou , V. & Karydas, A. -. G., 2016. A simple calibration procedure of polycapillary based portable micro-XRF spectrometers for reliable quantitative analysis of Cultural Heritage materials. *X-Ray Spectrometry* , pp. 85-91.

Kantarelou, V., 2016. *Development of the micro X- Ray Fluorescence Technique and its Analytical Applications for Cultural Heritage Artefacts, PhD Thesis.* Athens: s.n.

Kantarelou, V. & Karydas, A. G., 2016. A simple calibration procedure of polycapillary based portable micro-XRF spectrometers for reliable quantitative analysis of cultural heritage materials. *X-Ray Spectrometry*, March/April 2016, pp. 85-91.

Kantarelou, V., Karydas, A.-. G. & Sokaras, D., 2015. In situ scanning micro-XRF analyses of gilded bronze figurines at the National Museum of Damascus. *Journal of Analytical Atomic Spectroscopy*, June, Issue 30, pp. 1787-1798.

Kantarelou, V., Karydas, A. G. & Zarkadas, C., 2007. Micro-XRF Analysis of High Tin Bronze Mirrors at the Museum of Ancient Messene in Greece. In: V. Argyropoulos, A. Hein & M. A. Harith, eds. *Papers presented at the International Conference on Conservation Strategies for Saving Indoor Metallic Collections.* Cairo: s.n., pp. 93-99.

Kantarelou, V. et al., 2007. A novel approach on the combined in-situ application of LIBS and μ-XRF spectrometers for the characterization of copper alloy corrosion products. *METAL 07 Innovative investigation of metal artefacts*, pp. 35-41.

Karydas, A. -. G., 2007. Application of a Portable XRF Spectrometer for the Non-Invasive Analysis of Museum Metal Artifacts. *Annali di Chimica*, pp. 419-432.

Kregsamer, P., 2009. *QXAS- Quantitative X-ray analysis system (User's manual and guide to X-ray fluorescence technique,* Seibersdorf: XRF Group IAEA Laboratories Seibersdorf.

Liritzis, I. & Zacharias, N., 2011. Portable XRF of Archaeological Artifacts: Current Research, Potentials and Limitations. In: S. Shackley , ed. *X-Ray Fluorescence Spectroscopy (XRF) in Geoarchaeology.* New York: Springer.

Martini, M. &. S. E., 2006. s.l.:s.n.

Mattusch , C., 2006. Archaic and Classical Bronzes. In: O. Palagia, ed. *Greek Sculpture. Function, Materials, and Techniques in the Archaic and Classical Periods.* Cambridge: Cambridge University Press, pp. 208-242.

Mattusch, C., 1980. The Berlin Foundry Cup: The Casting of Greek Bronze Statuary in the Early Fifth Century B.C.. *American Journal of Archaeology*, 84(4), pp. 435-444.

Mattusch, C., 1988. *Greek Bronze Statuary. From the Beginnings through the Fifth Century B.C.* Ithaca & London: Cornell University Press.

Mattusch, C., 1988. *Greek Bronze Statuary. From the Beginnings through the the Fifth Century B.C.* Ithaca & London: Cornell University Press.

Muhly, J., 1985. Sources of Tin and the Beginnings of Bronze Metallurgy. *American Journal of Archaeology*, April, 89(2), pp. 275-291.

Philios, D., 1899. Bronze statue from Boeotia. *Archaeological Journal*, pp. 60-74.

Ridgway, B., 1984. *Roman copies of greek sculpture. The problem of the original.* Ann Arbor: University of Michigan Press.

Robertson, M., 1975. *A History of Greek Art.* 1st ed. London: Cambridge University Press.

Scott, D., 2002. *Copper and Bronze in art. Corrosion, colorants, conservation.* Los Angeles: Getty Publications.

Shugar , A. & Mass, L., 2012. *Handheld XRF for art and archaeology.* Leuven: Leuven University Press.

Symeonoglou, S., 1985. *The topography of Thebes from the Bronze Age to Modern Times.* New Jersey: Princeton University Press.

Van Grieken , R. & Markowicz, A., 2002. *Handbook of X-Ray Spectrometry.* 2nd edition ed. New York: Marcel Dekker .

Varoufakis, G., 1965. *Contribution in the research of corrosion in ancient bronzes/Συμβολή εις την έρευναν της διαβρώσεως αρχαίων βρούντζων.* Athens: s.n.

<table>
<tbody>
<tr><td colspan="10" align="center">Table 7. Qualitative results of all the areas analyzed</td></tr>
</tbody>
</table>
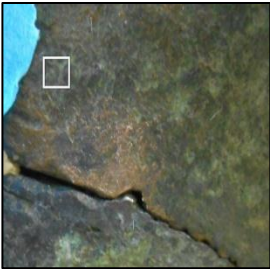
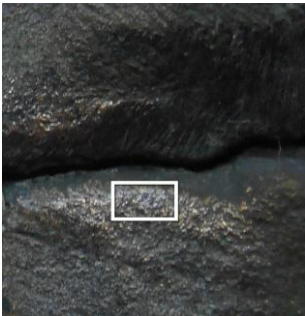| Photo | Name – Description of the area *Head* | Type of scan / Number of mea/ts / Time per step (s) / Area (mm^2) / Step (mm) / Filtered (F) or Unfiltered (U) | Elements detected (Counts per second) ||||||| |
|---|---|---|---|---|---|---|---|---|---|
| | | | Mn | Fe | Cu | Zn | As | Sn | Pb |
| | **Ba1** (back of the head / copper plating) | Area scan 10 /20 / 0.16 / 0.10 / F | 0.725 (detection limit) | 0.85 ± 0.26 | 9275 ± 846 | 22.5 ± 8.44 | 0.39 ± 0.276 | 2.505 ± 0.91 | 0.908 ± 0.191 |
| | **1a1** (back of the neck) – area of golden hue | Area scan 30 / 20 / 0.25 / 0.10 / F | 1.665 ± 0.593 | 8.026 ± 4.49 | 2903 ± 769 | 24.9 ± 11.1 | 21.1 ± 5.58 | 47.6 ± 6.53 | 29.5 ± 6.53 |
| | **1a2** (back of the neck) | Area scan 30 / 20 / 0.25 / 0.10 / F | 0.862 ± 0.264 | 3.48± 1.02 | 3097 ± 496 | 24.9 ± 3.35 | 17 ± 6.1 | 43.8 ± 5.97 | 24.2 ± 5.5 |
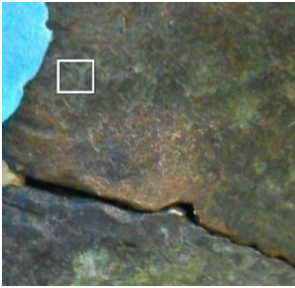
Photo	Name – Area *Head*	Type of scan / Number of mea/ts / Time per step (s) / Area (mm^2) / Step (mm) / Filtered (F) or Unfiltered (U)	Elements detected (Counts per second)						
			Mn	Fe	Cu	Zn	As	Sn	Pb
	1a3 (back of the neck) – area of black/grey color	Area scan 30 / 20 / 0.25 / 0.10 / U	25.5 ± 6.12	68.05 ± 15.3	28659 ± 4328	360.033± 102.5	107 ± 26.7	74.6 ± 13.3	80.35 ± 19.4
	3a1 (left eyebrow / inlaid)	Area scan 9 / 20 / 0.01 / 0.10 / F	0.616 (detection limit)	10.1 ± 2.88	5945 ± 3165	21 ± 10.07	13.2 ± 7.17	1.03± 0.467	6.96 ± 2.47
	4a1 (lower lip / inlaid)	Area scan 25 / 20 / 0.16 / 0.10 / F	0.386 (detection limit)	7.46 ± 2.57	7051 ± 2079	27.2 ± 14.9	20.18 ± 7.23	2.21 ± 0.842	10.7 ± 3.78

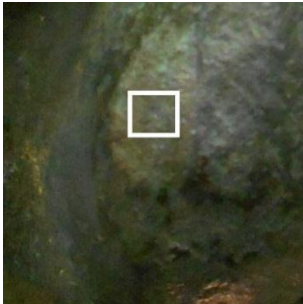| Photo	Name – Area *Head*	Type of scan / Number of mea/ts / Time per step (s) / Area (mm²) / Step (mm) / Filtered (F) or Unfiltered (U)	Elements detected (Counts per second)						
			Mn	Fe	Cu	Zn	As	Sn	Pb
	5a1 (nose) – area of green color	Area scan 12 / 20 / 0.09 / 0.10 / F	1.141 (detection limit)	4.67 ± 1.6	3432 ± 964	38.1 ± 12.7	18.8 ± 5.39	30.78 ± 2.19	15.4 ± 5.21
	5a2 (nose) – area of green color	Area scan 9 / 20 / 0.04 / 0.10 / F	1.127 (detection limit)	4.4 ± 0.809	5358± 435	35.3± 15.6	27± 3.43	37.1 ± 3.90	14.3 ± 3.09
	6a1 (upper left chest) – area of golden color	Area scan 12 / 20 / 0.24 / 0.20 / F	1.2 (detection limit)	15.8 ± 3.36	3710 ± 997	89.2 ± 39.01	11.03± 6.06	64 ± 9.8	46.9 ± 17.6

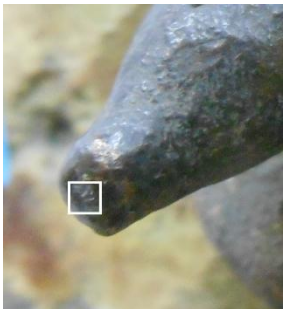| Photo	Name – Area *Upper body*	Type of scan / Number of mea/ts / Time per step (s) / Area (mm^2) / Step (mm) / Filtered (F) or Unfiltered (U)	Elements detected (Counts per second)						
			Mn	Fe	Cu	Zn	As	Sn	Pb
	11a1 (center of the chest) – area of golden color	Area scan 9 / 20 / 0.04 / 0.10 / F	1.4 (detection limit)	12.21 ± 1.34	6301 ± 944	27.7 ± 22.3	11.5 ± 5.99	43.9 ± 16.2	20.42 ± 11.4
	11a2 (center of the chest) – area of golden color	Area scan 9 / 20 / 0.04 / 0.10 / U	20.8 (detection limit)	187 ± 14.3	51792 ± 5885	255 ± 179	65.03 ± 19.1	74 ± 10.1	58.1 ± 38.8
	11a3 (center of the chest) – area of black/grey color	Area scan 9 / 20 / 0.04 / 0.10 / U	35.3 ± 2.25	338 ± 32.2	38063 ± 1946	949 ± 95	134 ± 12.2	99.7 ± 8.4	145 ± 12.9

Photo	Name – Area *Upper body*	Type of scan / Number of mea/ts / Time per step (s) / Area (mm²) / Step (mm) / Filtered (F) or Unfiltered (U)	Elements detected (Counts per second)						
			Mn	Fe	Cu	Zn	As	Sn	Pb
	11a4 (center of the chest) – area of black/grey color	Area scan 9 / 20 / 0.04 / 0.10 / F	1.67 ± 0.387	21 ± 1.65	4740± 683	104 ± 13.3	18.8 ± 4.02	63± 6.52	47.06 ± 7.58
	2a1 (back) – area of golden color	Area scan 15 / 20 / 0.08 / 0.10 / F	0.786 ± 0.272	11.08 ± 2.55	3753 ± 688	81 ± 25.4	12.04 ± 3.64	49.15± 9.44	34.3 ± 13.3
	Ma (back / Pb filling)	Area scan 12 / 20 / 0.06 / 0.10 / F	0.325 (detection limit)	0.33	0.39	13.4	6.31	nd	2886± 58.3

Photo	Name – Area *Genitalia*	Type of scan / Number of mea/ts / Time per step (s) / Area (mm^2) / Step (mm) / Filtered (F) or Unfiltered (U)	Elements detected (Counts per second)						
			Mn	Fe	Cu	Zn	As	Sn	Pb
	12a1 (left testicle) – area of green color	Area scan 4 / 20 / 0.09 / 0.10 / F	0.85 ± 0.141	2.13 ± 0.977	2208 ± 900	46.3 ± 20.8	11.3 ± 1.7	59.3 ± 12.5	8.89 ± 2.83
	12a2 (left testicle) – area of green color	Area scan 4 / 20 / 0.09 / 0.10 / U	27.6 ± 8.2	72.2 ± 14.7	19030 ± 2877	523.75 ± 55.9	83.7 ± 17.3	118 ± 18.1	82.3 ± 21.7
	14a1a (tip of the penis) – area of brown color	Area scan 4 / 20 / 0.01 / 0.10 / F	0.725 ± 0.087	58.6 ± 58.4	2955 ± 801	28.8 ± 9.14	12.3 ± 3.72	28.2 ± 3.85	11.2 ± 3.03

Photo	Name – Area *Genitalia*	Type of scan / Number of mea/ts / Time per step (s) / Area (mm^2) / Step (mm) / Filtered (F) or Unfiltered (U)	Elements detected (Counts per second)						
			Mn	Fe	Cu	Zn	As	Sn	Pb
	14a2 (tip of the penis) – area of brown color	Area scan 4 / 20 / 0.01 / 0.10 / U	47.5 ± 36.3	8210 ± 7904	17098 ± 11078	203 ± 77.4	53.2± 29.7	52.6 ± 11.8	32.7± 6.97
	15a1 (pubic hair) – area of brown color	Single spot / 20 / U	27.4	372	49372	774	9.5	37.703	1545
	15a2 (pubic hair) – area of brown color	Single spot / 20 / F	2	22.6	7829	73	38.2	12.7	6.71

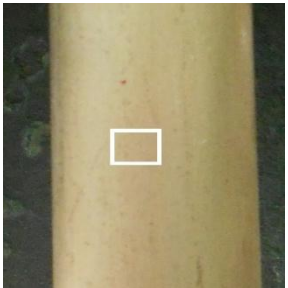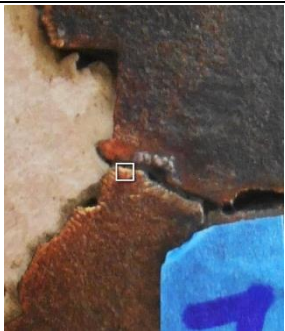| Photo	Name – Area *Right leg*	Type of scan / Number of mea/ts / Time per step (s) / Area (mm^2) / Step (mm) / Filtered (F) or Unfiltered (U)	Elements detected (Counts per second)						
			Mn	Fe	Cu	Zn	As	Sn	Pb
	8a1 (right thigh) – area of golden color	Area scan 12 / 20 / 0.09 / 0.10 / F	0.558 ± 0.034	9.28 ± 2.91	6249 ± 947	15 ± 4.78	15.4± 5.99	30.03 ± 17.9	14.2 ± 7.95
	8a2 (right thigh) – area of golden color	Area scan 12 / 20 / 0.09 / 0.10 / F	0.562 ± 0.112	9.83 ± 1.83	6567 ± 599	15.416 ± 5.32	15.1 ± 6.26	39.7 ± 6.85	12.3 ± 7.38
	8a3 (right thigh) – area of black color	Area scan 12 / 20 / 0.09 / 0.10 / F	1.183 (detection limit)	12 ± 3.18	3950 ± 737	45.3 ± 23.6	32.9 ± 11.4	56.2 ± 6.67	37 ± 15.8

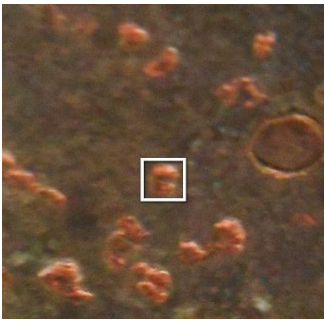| Photo	Name – Area *Right leg*	Type of scan / Number of mea/ts / Time per step (s) / Area (mm^2) / Step (mm) / Filtered (F) or Unfiltered (U)	Elements detected (Counts per second)						
			Mn	Fe	Cu	Zn	As	Sn	Pb
	8a4 (right thigh)	Area scan 12 / 50 / 0.09 / 0.10 / U	20.7± 3.15	182 ± 36.2	33960 ± 4780	456 ± 230	194.3 ± 60.7	94.5 ± 11.5	118 ± 48.2
	8a5 (right thigh / white area)	Area scan 12 / 50 / 0.06 / 0.10 / U	43.7± 6.6	323 ± 38.1	11367 ± 8344	101 ± 44.6	224 ± 54.1	253± 21.6	399 ± 85.8
	8a6 (right thigh) area of white color	Area scan 12 / 20 / 0.06 / 0.10 / F	1.33 ± 0.143	15.8 ± 1.9	491 ± 362	45 ± 25	20.6 ± 4.46	127 ± 7.1	117 ± 18.4

Photo	Name – Area *Leg*	Type of scan / Number of mea/ts / Time per step (s) / Area (mm^2) / Step (mm) / Filtered (F) or Unfiltered (U)	Elements detected (Counts per second)						
			Mn	Fe	Cu	Zn	As	Sn	Pb
	13a1 (axis of support / right leg)	Area scan 12 / 20 / 0.24 / 0.20 / F	nd	nd	4489 ± 106	2421 ± 61.9	nd	nd	47.93± 6.3
	7a1a (left leg) – area of golden color	Area scan 4 / 20 / 0.01 / 0.10 / F	1.012 ± (detection limit)	12.5 ± 3.14	7126 ± 652	60.3 ± 48.5	12.6 ± 1.78	1.6 ± 0.74	25.5 ± 6.48
	7a2 (left leg) – area of golden color	Area scan 4 / 20 / 0.01 / 0.10 / F	0.987 ± (detection limit)	9.71± 2.038	6587 ± 886	29.8 ± 11	13 ± 3.55	24.9± 13.2	20.4 ± 16.6

Photo	Name – Area *Left leg*	Type of scan / Number of mea/ts / Time per step (s) / Area (mm²) / Step (mm) / Filtered (F) or Unfiltered (U)	Elements detected (Counts per second)						
			Mn	Fe	Cu	Zn	As	Sn	Pb
	Aa1 (copper plating)	Area scan 9 / 20 / 0.01 / 0.10 / F	nd	0.933± 0.514	5127 ± 1781	15.2 ± 5.7	1.3 ± 0.644	nd	0.725 ± 0.268
	9a1 (foot) – area of golden color	Area scan 12 / 20 / 0.06 / 0.10 / F	0.32 ± 0.097	11.02 ± 2.47	2033± 1305	41.5 ± 14.2	12 ± 4.98	43.3 ± 10.4	40.4 ± 19.4
	9a2 (foot) – area of golden color	Area scan 25 / 20 / 0.16 / 0.10 / F	0.406 ± (detection limit)	9.408 ± 2.043	2300 ± 755	37.7 ± 11.2	14.6 ± 5.35	46.7 ± 7.96	42.4 ± 17

Photo	Name – Area *Left leg*	Type of scan / Number of mea/ts / Time per step (s) / Area (mm^2) / Step (mm) / Filtered (F) or Unfiltered (U)	Elements detected (Counts per second)						
			Mn	Fe	Cu	Zn	As	Sn	Pb
	9a3 (foot) - area of black color	Area scan 12 / 20 / 0.09 / 0.10 / F	0.312 ± 0.043	10.3 ± 3.068	1828 ± 645	80 ± 17.4	84.5 ± 36.9	7.53 ± 0.74	50.5 ± 8.84
	9a4 (foot) - area of black color	Area scan 12 / 20 / 0.09 / 0.10 / U	11.08 ± 2.137	196 ± 37.4	18698 ± 4502	808 ± 164	83.2 ± 18.1	149 ± 23.6	166 ± 50.3
	10a1 (base) - area of golden color	Area scan 9 / 20 / 0.09 / 0.10 / F	0.983± 0.182	22.09 ± 11.4	3540± 1117	32 ± 12.4	24.1± 6.62	45.5 ± 9.34	38.8 ± 10.02

			Concentration of elements detected (in % w/w) with standard deviation in % of the characteristic X-ray intensities during area scans						
Photo	**Name – Area**	**Type of scan / Number of mea/ts / Time per step (s) / Area (mm^2) / Step (mm) / Filtered (F) or Unfiltered (U)**	**Mn**	**Fe**	**Cu**	**Zn**	**As**	**Sn**	**Pb**
	Ba1 (copper plating / back of the head)	Area scan 10 / 20 / 0.16 / 0.10 / F	0.012 (detection limit)	0.0091 ± 0.0027	98.9 ± 9.02	0.18 ± 0.068	0.013 ± 0.005	0.884 ± 0.32	0.0165 ± 0.007
	Aa1 (copper plating / left leg)	Area scan 9 / 20 / 0.01 / 0.10 / F	0.016 (detection limit)	0.018 ± 55.1	99.7± 34.7	0.223 ± 37.4	0.037 ± 44.5	nd	0.04 ± 41.9

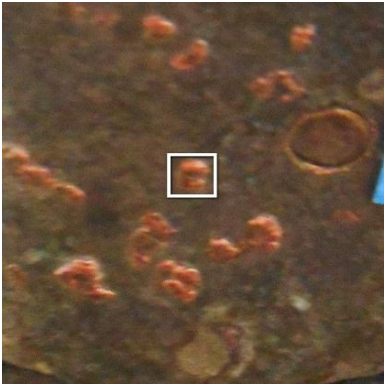**Table 8. Quantitative results of selected areas**

Photo	Name – Area *Face*	Type of scan / Number of mea/ts / Time per step (s) / Area (mm^2) / Step (mm) / Filtered (F) or Unfiltered (U)	Concentration of elements detected (in % w/w) with standard deviation in % of the characteristic X-ray intensities during area scans						
			Mn	Fe	Cu	Zn	As	Sn	Pb
	4a1 (lower lip / inlaid)	Area scan 25 / 20 / 0.16 / 0.10 / F	0.008 D.L	0.105 ± 34.5	98 ± 29.5	0.285± 54.7	0.493 ± 35.2	1.014 ± 38.1	0.083 ± 35.7
	3a1 (left eyebrow / inlaid)	Area scan 9 / 20 / 0.01 / 0.10 / F	0.015 D.L	0.167 ± 28.5	98.3 ± 53.2	0.261 ± 48	0.316 ± 58.8	0.566 ± 45.3	0.326 ± 44.2

Photo	Name – Area *Legs*	Type of scan / Number of mea/ts / Time per step (s) / Area (mm^2) / Step (mm) / Filtered (F) or Unfiltered (U)	Concentration of elements detected (in % w/w) with standard deviation in % of the characteristic X-ray intensities during area scans						
			Mn	Fe	Cu	Zn	As	Sn	Pb
	8a1 (right thigh)	Area scan 12 / 20 / 0.09 / 0.10 / F	0.015 D.L.	0.17 ± 31.4	86.9 ± 15.1	0.15 ± 31.9	0.157 ± 35.6	11.7 ± 59.5	0.875 ± 46.6
	7a2 (left leg)	Area scan 4 / 20 / 0.01 / 0.10 / F	0.025 D.L.	0.165± 21	88.5 ± 13.5	0.3 ± 36.8	0.106 ± 29.6	9.67± 53.1	1.28 ± 60.6